March 2016

Fluid Flow Distribution Control in Micro-Scale with EHD Conduction Pumping Mechanism

Omesh Keshav Kamat
Worcester Polytechnic Institute

Thomas Rae Larkin
Worcester Polytechnic Institute

Tobin James Dancy
Worcester Polytechnic Institute

Fluid Flow Distribution Control in Micro-Scale with EHD Conduction Pumping Mechanism

A Major Qualifying Project Report

submitted to the Faculty

of the

WORCESTER POLYTECHNIC INSTITUTE

in partial fulfillment of the requirements for the

Degree of Bachelor of Science

By

Tobin Dancy

Omesh Kamat

Tommy Larkin

Submitted:
3/25/16

Project Advisor:

Dr. Jamal Seyed-Yagoobi

Abstract

Electrohydrodynamic (EHD) conduction pumping technology utilizes the interaction between an applied electrical field and dissociated ions within a dielectric fluid to generate a net body force within the working fluid, which results in a net flow in a desired direction. EHD conduction pumps have noticeable benefits when compared to their traditional mechanical counterparts due to their low vibration and noise generation, low power consumption, and ability to operate in microgravity. EHD conduction pumps provide intelligent flow control via their ability to vary the electric field voltage applied to their electrodes. Flow distribution control using EHD conduction pumps has been previously examined in macro- and meso-scale configurations confirming effective redistribution of flow and recovery from mal-distribution in both single and two-phase flows. The purpose of this Major Qualifying Project was to study the use of EHD conduction pumps in controlling single phase flow distribution through parallel micro-channels, 500 microns tall, using upstream micro-scale EHD pumps. Voltage applied to the micro-scale EHD conduction pumps ranged between 0-1500 volts. The working fluid used in these experiments was the refrigerant HCFC-123, operated at ambient conditions.

Acknowledgements

We would like to first thank Worcester Polytechnic Institute and the Mechanical Engineering Department at WPI for providing us with the technological and financial resources, as well as the educational background, required to complete this project. The team would like to offer special thanks to Michal Talmor and Lei Yang, the PhD students in WPI's Multi-Scale Heat Transfer Laboratory, for their never ending support and guidance throughout each step of this project. Most of all, we would like to thank Professor Jamal Seyed-Yagoobi for advising the project and providing us with guidance and encouragement throughout the process. We would also like to thank David Richard and Andrew Barakos of Nova Biomedical for their assistance in the manufacturing of our evaporator assembly. Lastly, we would like to acknowledge the professional vendors we have had the pleasure to work with: McMaster-Carr, Speedy Metals, Ultimate Plastics, and Omega.

Table of Contents

Abstract 2
Acknowledgements 3
Table of Contents 4
Table of Figures 8
Table of Tables 9
Chapter 1: Introduction 10
1.1 Overview of Electrohydrodynamics 10
1.2 Project Overview 12
1.3 Primary EHD Pumping Mechanisms 13
1.3.1 Ion-Drag Pumping 13
1.3.2 Induction Pumping 14
1.3.3 Conduction Pumping 14
1.4 Potential Applications 16
Chapter 2: Methodology and Experimental Setup 18
2.1 Overview 18
2.2 Requirements 18
2.3 Design 20
2.3.1 EHD Conduction Pump 21
2.3.2 Evaporator Design 21
Constraints 22
Initial Design 23
Final Design 25
2.3.3 Initial Calculations 28
Pressure Drop 28
Evaporator Heat Transfer 31
Condenser Length 33
2.4 Evaporator Manufacturing 36
2.5 Experimental Loop Assembly 37
2.5.1 Evaporator 38
Prepping the EHD Pump 40

Powering the EHD Pump 41
Prepping for the Evaporator 43
Manifolds 44
2.5.2 Condenser 46
2.5.3 Mechanical Pump 46
2.5.4 Reservoir 47
2.6 Sensors Configuration and Calibration 48
2.6.1 Flowmeters 49
2.6.2 Differential Pressure Transducers 51
2.6.3 Absolute Pressure Transducer 53
2.6.4 Thermocouple Probes 53
2.7 Data Acquisition 54
2.7.1 Electrical and Grounding 54
2.7.2 LabVIEW 56
2.8 Experimental Preparation 57
2.8.1 Leak Testing 57
2.8.2 Methods of Leak Testing 58
2.8.3 Methods of Leak Correction 59
2.8.4 Charging the Reservoir 59
2.8.5 Pulling a Vacuum 61
2.8.6 Filling the Experimental Loop 62
Experimental Matrix 63
Variable Conditions and Ranges 64
Basic Experimental Procedure 64
Experiment I: Static Condition 65
Experiment II: Pump Performance 65
Experiment II: Equal Distribution to Maldistribution 66
Experiment III: Maldistribution to Equal Distribution 67
Chapter 3: Results and Discussion 68
3.1 Experiment I: Static Conditions 68
3.2 Experiment II: Dynamic Pump Performance Test 69
3.3 Experiment III: Equal Flow to Maldistribution 70
3.4 Experiment IV: Maldistribution to Equal Distribution 72

3.5 Potential Causes of Error 72
Conclusion 74
References 75
Appendices 77
Appendix A: Assembly Loop Solid Models 77
Full Loop Assembly 77
Section 1: Evaporator Side 77
Section 1: Evaporator Side – EHD Pumps 78
Section 1: Evaporator Side – Flowmeters 78
Section 1: Evaporator Side – Evaporator 79
Appendix B.1: Differential Pressure Transducers Calibration Curves 80
Differential Pressure Transducer 1 80
Differential Pressure Transducer 2 80
Differential Pressure Transducer 3 81
Differential Pressure Transducer 4 81
Appendix B.2: Flowmeters Calibration Curves 82
Flowmeter 1 82
Flowmeter 2 82
Appendix C.1: LabVIEW Block Diagram 83
Appendix C.2: LabVIEW User Interface 84
Appendix D.1: Thermocouple Probe Configuration 85
Appendix D.2: Flowmeters Configuration 85
Appendix D.3: Differential Pressure Transducers Configuration 85
Appendix D.4: EHD Pump Voltage/Current Supply Configuration 85
Appendix E.1: Experimental Test Curves 86
Static Condition – Trial 1 86
Static Condition – Trial 2 86
Static Condition – Trial 3 87
Pump Performance – Trial 2 87
Static Condition – Trial 3 88
Equal Distribution to Maldistribution 88
Appendix F: Physical Properties of R-123 89
Appendix G.1: Loop Pressure Drop MATLAB Calculations 90

Appendix G.2: Evaporator Pressure Drop MATLAB Calculations..... 93
Appendix G.3: Length of Condenser MATLAB Calculations 98

Table of Figures

Figure 1: Dissociation and Recombination of Molecules. 15
Figure 2: Formation of Heterocharge Layers [1]. 15
Figure 3: EHD Conduction Electrode Configuration [8]. 16
Figure 4: Loop Assembly Schematic. 20
Figure 5: EHD Conduction Pump with Electrodes [14]. 21
Figure 6: Initial Micro-channel Chip Model. 23
Figure 7: Initial Evaporator Assembly Model. 24
Figure 8: Final Teflon Micro-channel Chip Model. 25
Figure 9: Final Evaporator Assembly Model. 27
Figure 10: Moody diagram [9]. 30
Figure 11: Hi-Density Cartridge Heater (Omega). 32
Figure 12: Evaporator - Conduction heat transfer. 33
Figure 13: Top overview of the experimental setup. 38
Figure 14: Differential pressure transducers configuration. 39
Figure 15: Cleaning of the EHD Pumps. 40
Figure 16: Checking connection of electrodes to bus lines. 41
Figure 17: High voltage feedthroughs. 42
Figure 18: Complete assembly of the EHD pumps. 43
Figure 19: Manual tube bender. 44
Figure 20: Manifold attached to the evaporator section. 45
Figure 21: Condenser section. 46
Figure 22: Mechanical pump section. 47
Figure 23: Reservoir section. 48
Figure 24: Sensirion flowmeters. 49
Figure 25: Calibration of Flowmeter 1. 50
Figure 26: Differential pressure transducer calibration apparatus. 51
Figure 27: Calibration of a Differential Pressure Transducer. 52
Figure 28: DAQ Board. 55
Figure 29: Conductivity testing for grounding. 56
Figure 30: Underwater leak testing method. 58
Figure 31: Elevated R-123 tank for filling the reservoir. 61
Figure 32: Genco HYVAC 7 pulling a vacuum. 62
Figure 33: Static Condition: EHD Voltage vs. Differential Pressure across Branch 2, Trial 3 68
Figure 34: Pump Performance Curve: EHD Voltage vs. Pump Performance (mL/min) in Branch 2, Trial 3 69
Figure 35: Pump Performance Curve, EHD Voltage vs. Differential Pressure in Branch 2, Trial 3 70
Figure 36: Flow Distribution, Equal to Maldistribution: EHD Voltage vs. Differential Pressures in Branch 1&2 71
Figure 37: Flow Distribution: Equal to Maldistribution, EHD Voltage vs. Flow Rate (mL/min) in Branches 1 & 2 71

Table of Tables

Table 1: Pressure drop and flow rates through each section. 31
Table 2: Temperature of Condenser vs. Length. 35
Table 3: Locations of the Thermocouple Probes. 54
Table 4: Experimental Variables. 63
Table 5: Pump Performance Experimental Matrix. 65
Table 6: Pump Performance Experimental Matrix. 65
Table 7: Equal to Maldistribution Experimental Matrix. 66
Table 8: Mal to Equal Distribution Experimental Matrix. 67

Chapter 1: Introduction

1.1 Overview of Electrohydrodynamics

Electrohydrodynamics, abbreviated as EHD, is the study of interactions between applied electrical fields and fluid flow fields. EHD technology is most prevalently used for pumping, in which the application of an electric field on a working fluid is capable of generating net flow. The three main types of EHD pumping which are enacted primarily by the Coulomb force are ion-drag, induction, and conduction pumping, which vary in their methods of inducing charge in the working fluid. The focus on this project is on EHD conduction pumping.

The physics behind EHD pumping identifies three main forces which are most involved in the interactions between the applied electric field and the working fluid, and which result in a net force applied to the fluid causing its motion. These EHD forces which are imposed on the fluid are the Coulomb, Dielectrophoretic (DEP), and Electrostriction forces, the sum of which is referred to as the net body force, described by the net body equation as seen below [2].

$$\overrightarrow{F_E} = q\vec{E} - \frac{1}{2}E^2\nabla\epsilon + \nabla[\rho\frac{E^2}{2}\left(\frac{\partial\epsilon}{\partial\rho}\right)_T]$$

Coulomb's Law relates the Coulomb force on a point charge (F), to the charge density of the particle (q), and the strength of an applied electric field (E). This relationship is directly proportional between the strength of the electric field and the body force on the particle such that an increase in the applied electric field strength results in a higher force on the particle. This is expressed mathematically by the equation:

$$F = qE$$

The DEP force is determined by an applied electric field's strength and a gradient of the fluid's property known as permittivity, denoted as ϵ, which describes an electromagnetic

medium's resistance to an applied electric field. In an isothermal application there is no gradient in the working fluid's permittivity [1], such that the DEP force term is negligible in single phase fluid applications.

The electrostriction force is dependent on the permittivity of the working fluid as well as the fluid's mass density (ρ), and the differential of the fluid's permittivity against its mass density as determined at a constant temperature. In a similar manner as the DEP force, single phase isothermal applications do not experience permittivity gradients or significant changes in density [3]. Thus the electrostriction force contributes to fluid flow on such a small level that it can be neglected for single phase fluid applications, such that the net force felt by the fluid is only significantly a result of the Coulomb force. Consequently in EHD experiments using isothermal single phase fluid, such as those conducted for this report, the net body force equation can be simplified as:

$$\overrightarrow{F_E} = q\vec{E}$$

1.2 Project Overview

The purpose of this Major Qualifying Project was to study the use of EHD conduction pumps in controlling flow distribution through parallel micro-channels using micro-scale EHD pumps. This project also sought to the pave way for future research in observing the heat transfer capabilities of EHD conduction driven flow through micro-channels and the impact on flow distribution control for applications in which the working fluid experiences phase change. A two-phase capable loop assembly was designed and constructed in order to study the generation of flow and pressure via the micro-scale EHD conduction pumps.

There are several advantages of EHD conduction pumps when compared to standard mechanical pumps. These pumps consume low amounts of power as they utilize high voltages but very low currents typically on the order of five hundred microamps or less, they require little to no maintenance, are extremely lightweight, and involve no moving parts which avoids the significant generation of noise and vibrations found in typical mechanical pumps. EHD conduction pumps provide smart flow control in their systems via their ability to vary the electric field voltage applied to their electrodes. The pumps are effective in both single and two-phase flow conditions [1] and also have the ability to operate in microgravity conditions due to their operational independence from gravity [5] which makes them especially well-suited to aerospace applications.

The results and conclusions from this study could directly impact a wide range of engineering applications in fields which micro-scale EHD technology could revolutionize, particularly the booming aerospace and electronics industries. The micro-scale EHD conduction pumping studied in this project has huge potential to increase performance and efficiency in

applications like microelectronics cooling, thermofluid system flow regulation, and low-gravity heat transfer enhancement.

1.3 Primary EHD Pumping Mechanisms

EHD pumping is achieved by applying an electric field to a dielectric working fluid so as to achieve a net flow. There are three primary types of EHD pumping which are distinguished by the method in which charges are introduced to the working fluid. Each technique is capable of different levels of pressure generation and can be suitable to various applications; additionally each has its own associated benefits and drawbacks.

1.3.1 Ion-Drag Pumping

The first EHD flow generation phenomenon to be researched was EHD ion-drag pumping, the fundamentals of which centers on the fact that dielectric fluids can be pumped by the injection of ions, which has been known for more than one hundred years. Ion-drag pumping involves the use of a pair of electrodes, one of which is a sharp, charge-injecting source, referred to as an emitter, and the second which is an oppositely charged collecting electrode, referred to as a collector. When a strong electric field is established between this pair of electrodes, the corona effect causes a discharge of ions from the emitter. The injected ions are pulled through the fluid along the electrical field lines from the emitter towards the oppositely charged collecting electrode [1], generating flow as a result of the particle drag against the adjacent fluid. The major issues with the use of ion-drag pumping are primarily related to deterioration in the electrical properties of the working fluid and a dulling of the emitter electrode as it is discharged into the fluid. As the fluid's electrical properties deteriorate there is a significant drop in

efficiency as well as potential safety hazards related to continued operation of the pumping mechanism.

1.3.2 Induction Pumping

EHD induction pumping is a flow generation method which is based primarily on the Dielectrophoretic (DEP) force. As previously mentioned the DEP force is dependent upon a gradient in the permittivity of the working fluid, which is most commonly imposed by non-uniform thermal conditions or a change of phase in the fluid. The presence of these thermal gradients can induce gradient in electrical conductivity in different regions of the fluid, and therefore a net charge into the dielectric fluid, which when an AC electric wave is transmitted through the fluid will attract or repel the charges induced in the medium and generate flow. The frequency and voltage of the AC wave can be altered in order to change the flow velocity generated in the fluid. Applications of induction pumping include thin film pumping as well as enhanced heat transfer in two phase pumping scenarios [6]. Due to its need for thermal gradients, induction pumping is not suitable for isothermal applications such as those studied in this report.

1.3.3 Conduction Pumping

The pumping mechanism utilized as a part of this Major Qualifying Project is known as conduction pumping, which achieves flow by applying a high voltage electric field to a dielectric fluid across an asymmetrically organized set of electrodes. When affected by an electric field there is a dissociation and recombination of ions within the working fluid, as illustrated in the figure below, though under conditions of low electric field intensity these dielectric impurities in

the fluid separate and recombine at a relatively equivalent rate resulting in overall dynamic charge equilibrium within the fluid [4].

$$AB \underset{Recombination}{\overset{Dissociation}{\longleftrightarrow}} A^+ + B^-$$

Figure 1: Dissociation and Recombination of Molecules.

However as the voltage of the electric field is increased the rate of dissociation of ions also increases, such that at high voltage conditions the rate of dissociation is significantly greater than that of recombination, which results in non-equilibrium conditions. As these ions grow in numbers, they begin to form into layers on top each of the electrodes. The positively charged ions attract to the ground electrodes and the negatively charge ions attract to the positively charged high voltage electrodes. These layers of uniformly charged ions are referred to as heterocharge layers, as shown in Figure 2.

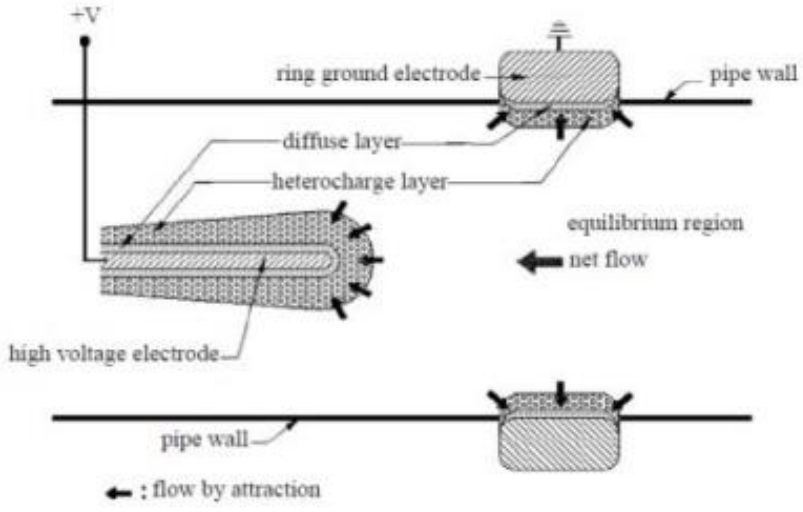

Figure 2: Formation of Heterocharge Layers [1].

In order to avoid a balancing of the Coulomb forces between the oppositely charged heterocharge layers, the high voltage electrodes are designed asymmetrically which builds up a significantly larger heterocharge layer and generates a net flow as ions drag fluid along as they move towards adjacent electrodes. A schematic of the flow direction is shown below.

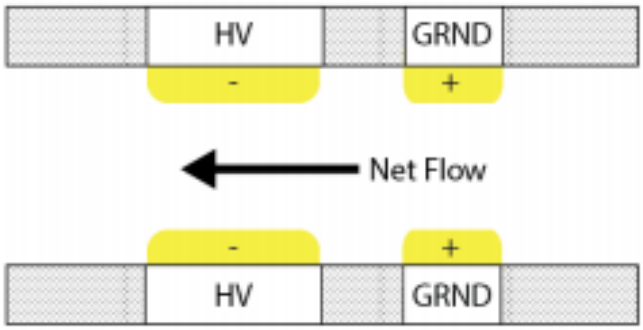

Figure 3: EHD Conduction Electrode Configuration [8].

EHD conduction pumping was chosen as the pumping mechanism for these experiments due to its pressure generation ability, durability, and proven efficiency in previously conducted experiments and studies. EHD conduction does not deteriorate the electrical properties of the working fluid since the dissociation and recombination processes are reversible, and no thermal gradients are required, making this a simpler mechanism to use for pumping.

1.4 Potential Applications

As previously stated there is a wide range of fields which EHD conduction pumping has the potential to revolutionize. There are several advantages to EHD conduction pumping with regards to flow control and distribution, as well as improving the efficiency of heat transfer. A primary advantage of EHD conduction pumping is its responsiveness with regards to the immediate impact of a change in applied voltage on flow velocity, as well as the ability to

operate effectively in multi-scale and low gravity environments. In cooling applications, particularly those at risk of dry-out, such as thin film coolant, the working fluid could be intelligently redistributed to match local heat transfer needs and preserve safe and efficient system operation.

The light and simple design of EHD pumping mechanisms involve no moving parts which drastically reduces the noise and vibrations typically created by mechanical pumps. EHD conduction pumps specifically have a very low current draw which results in low power consumption, and require little maintenance which makes them well suited to low-accessibility applications like those in space where dependable technology is critical. Most microelectronic cooling applications are currently limited by issues of scale and heat transfer efficiency, for both of which EHD pumping could be a suitable solution. Most working fluids currently used in thermal systems are refrigerant dielectrics, which could facilitate a very smooth transition towards flow control using EHD conduction pumping. Perhaps the largest drawback of EHD conduction pumping is the requirement of a high voltage electric field supply for operation, which poses risks and overall system design constraints, such as the proximity of other electronic components. Realistically at the current point in time, EHD conduction pumping is a very cutting-edge field of research and has not been studied to a point where a full scope of its capabilities and potential are understood and documented.

Chapter 2: Methodology and Experimental Setup

2.1 Overview

The main purpose of these experiments was to collect data on the capabilities of micro-scale EHD conduction pumping and flow distribution with parallel micro-channels in a two-phase loop. Initial testing completed during this project were for single phase performance only, but the experimental setup was designed and built to accommodate future two-phase tests. The experimental setup was designed for simulating heat transfer applications relating to micro-chips. Given current technology additional electronic elements cannot be added to micro-chips due to the very high heat flux generated by densely packed micro-transistors. EHD conduction pumping presents a potential solution to these cooling problems. Future two phase experiments using the assembly constructed as a part of this project may be designed to observe whether industry standards for micro-electronics cooling, using fluid evaporation for higher heat flux removal capabilities, can be met by EHD conduction pumping.

2.2 Requirements

In order to achieve the set project goals, specific requirements for the assembly design and construction were developed.

1. The experimental setup needed design elements based on the dimensional parameters of an actual electronic chip. The set dimension requirements dedicated chip length and width, as well as size of the micro-channels through which fluid would pass.
2. The experimental setup was required to complement the characteristics and constraints of the EHD pumps. Since the EHD pumps have a maximum pressure that they can generate, it was important design a loop which would not overwhelm the pumps. Based on

previous and ongoing experiments in the lab, it was apparent that a mechanical pump would be required to provide additional pressure generation in order to assist the EHD pumps, and in order to test flow redistribution of different initial flow conditions.

3. The experiments demanded flow distribution characteristics for a variety of different pumping configurations, requiring means of controlling channel flow by means of voltage applied to each pump and through use of valves to establish desired experimental conditions for each pumping configuration. The parallel EHD conductions would need to be able to operate both separately and simultaneously.
4. All electronic equipment, inputs, and sensors needed to be controllable through the use of LabVIEW Virtual Instrumentation software. Previous EHD experiments within the Multi-scale Heat Transfer Lab had used the same software, and it was determined to be the most easily available, consistent, and cost efficient solution.
5. The experiment had to yield meaningful data. By means of iterative and thorough design, well-planned means of data collection, careful calibration, and strict adherence to proper laboratory procedure, the acquisition of reliable data was expected.

In order to achieve all of the above requirements, the experimental setup needed to contain a variety of sensors, including differential and absolute pressure transducers, flowmeters, and thermal probes, while using data acquisition (DAQ) boards and LabVIEW as the user interface for the measurement, observation, and processing of data. The data collected by these methods, in the form of flow rates and pressures, provided valuable documentation of the performance and capabilities of the micro-scale EHD conduction pumps.

2.3 Design

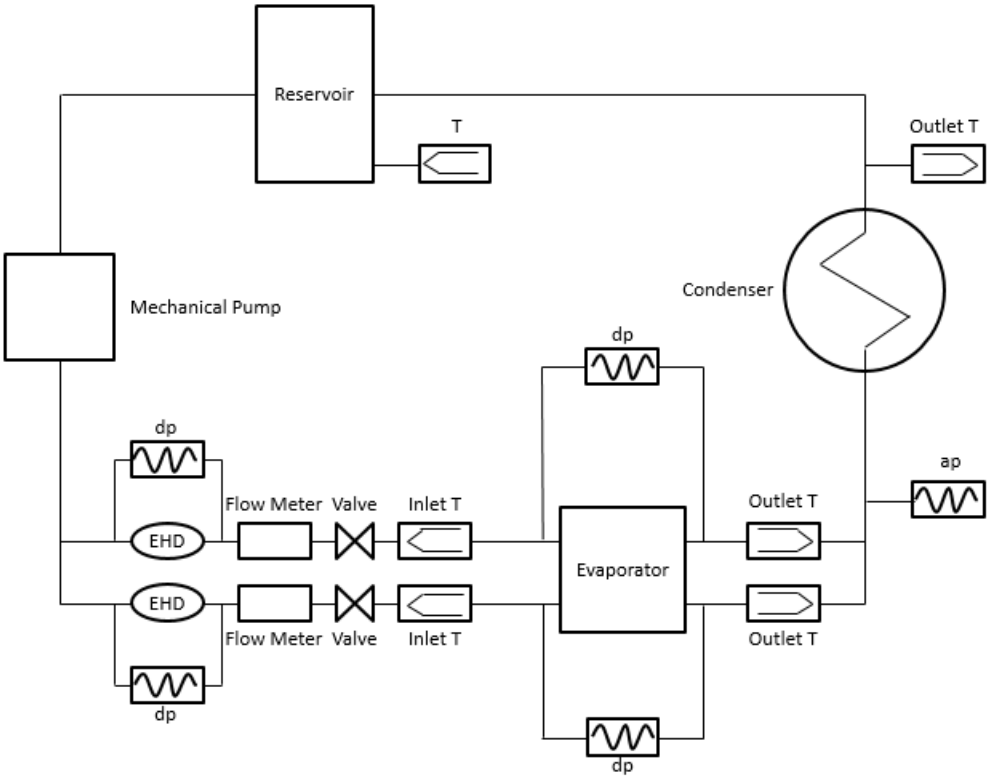

Figure 4: Loop Assembly Schematic.

The components of a loop necessary for experimenting in two phase include an evaporator, a condenser, a reservoir, valves, flow meter sensors, thermocouples, differential pressure transducers and absolute pressure transducers. Valves and flow meters are essential to control the flow rate within each branch. Each branch must be able to individually measure temperature and pressure change across key components such as the evaporator and EHD pumps. Temperature and differential pressure measurements are important across the evaporator to read and adjust to saturation temperature and pressure. A condenser is also important to bring the fluid back to the liquid phase. The selection for the EHD pumps in this loop setup was limited by operating pumps already found in the laboratory. Finally, the working fluid used for this loop was HCFC-123.

2.3.1 EHD Conduction Pump

The EHD Conduction pumps utilized in this experiment are comprised of twenty pairs of EHD electrodes. Fluid flows through a central hole of one millimeter diameter as it is pumped. There are additional holes on the perimeter of the electrode pairs for the bus lines which deliver power. The maximum pressure generation for this type of conduction pump is on the order of hundreds of Pascals.

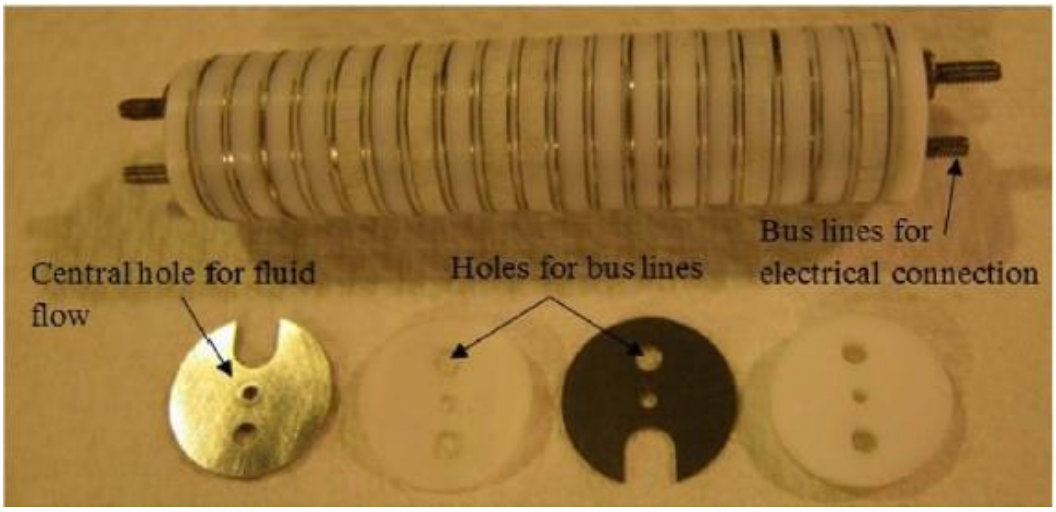

Figure 5: EHD Conduction Pump with Electrodes [14].

2.3.2 Evaporator Design

The most significant design challenge within the experimental setup was the design and manufacturability of the polytetrafluoroethylene (PTFE or Teflon) chip component of the evaporator assembly, which housed the dual parallel micro-channels. The chip dimensions were ten by ten millimeter, with the micro-channels each being only two millimeters wide and five hundred microns in depth. The evaporator pieces needed to be designed such that each micro-channel could be individually heated and fluid could still be transported throughout the rest of evaporator-condenser loop. Each micro-channel was connected to one of the parallel branches of the loop with its own upstream EHD conduction pump.

Constraints

One major design constraint was centered on designing manufacturable micro-channels which could be connected to the much larger loop branches without a harsh disruption of the fluid flow regime. The depth of the channels needed to be manufactured to within a five micron tolerance for accurate data, which was a tolerance that WPI manufacturing labs were not completely confident in. Rather than attempting to machine the evaporator parts using WPI CNC machines an outside company was contacted to provide assistance with achieving the required manufacturing precision.

The task of smoothly transitioning the flow from the large cylindrical inlet pipe nipples to the manufactured rectangular micro-channels required the design of a special tapering at the beginning and end of the micro-channels on the surface of a PTFE Teflon chip. The transition from cylindrical pipes to rectangular channels of a much smaller area would create undesirable pressure drops and possible turbulence. The taper which was designed to serve as the transition between channel sizes was manufactured with painstaking precision, making use of individual single steps with a 1/32nd inch bit to achieve the necessary taper angle.

Additionally, the entire assembly needed to be leak proof for both the integrity of the experiment and the general safety of those working in the lab. Any manufactured part needed to seal off any possible unintended flow outside of passages of the loop. In order to reduce leak, any connection between parts of the loop, including inlets and outlets of the channels, needed to be stainless steel.

The final imposed constraint was to deliver heat transfer separately to each channel. Each channel needed to be insulated, so that heat could not transfer between channels and was instead primarily transferred out through the convection of the fluid transport. The insulation constraint

meant the channels needed to be thermally resistant. A method to deliver heat along each channel also needed to be designed.

Initial Design

The initial manufacturing approach to creating micro-channels was to carve out the channels from a rectangular block of material. CNC machines at WPI had the capability able to mill away the channels close to the specific depth, length, and width, though there were some concerns on the accuracy of the high tolerance operations. The milling drills could not create 'slots' through the middle of a larger chip due the geometry of the drills, but could instead cut away material from the top and bottom half of the chip to create space for the channels.

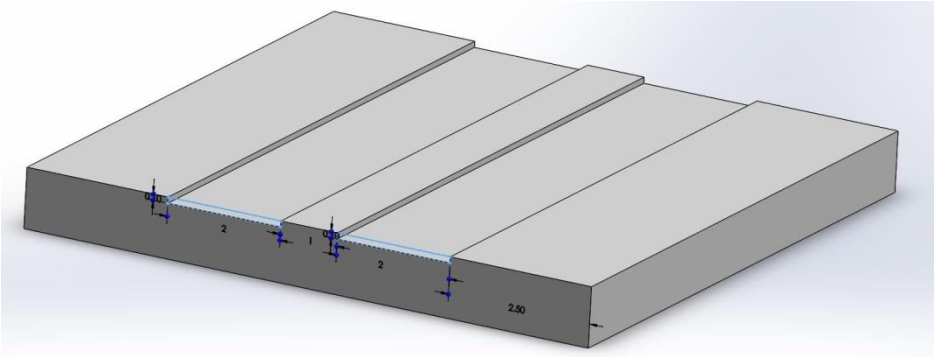

Figure 6: Initial Micro-channel Chip Model.

In the original design, a separated two piece manufactured box that would hold the chip with the channels inside is included. The box's top piece was designed to have lipped extrusion to compress the chip into place within the box's cavity. The lip would be fitted with a fluorocarbon material to cap the channels and prevent fluid from filling the rest of the cavity. The two pieces would seal together with bolts threaded from the top. This box had inlet and outlet holes for the tube fittings to slide into at locations where the channels would be located inside.

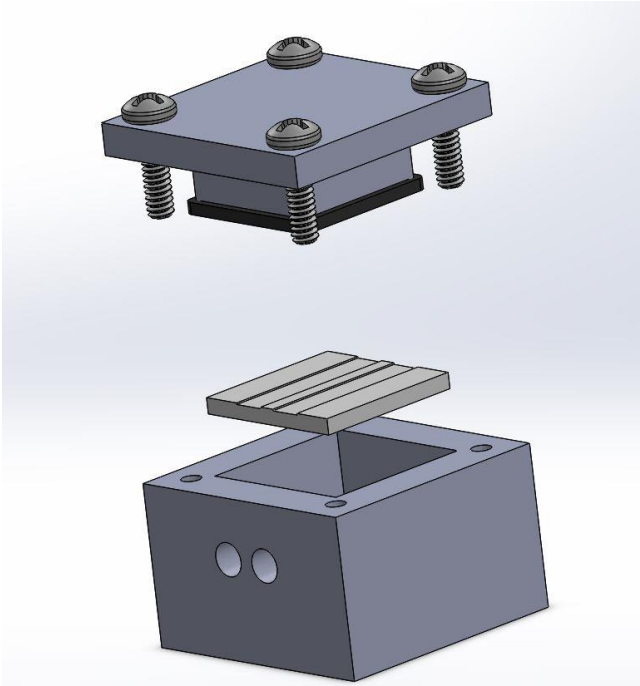

Figure 7: Initial Evaporator Assembly Model.

Final Design

The main revision to the design of the chip assembly was that this did not account for the tapering between the pipe fittings to the channels. At first the taper was within the inlet of the outer box, where a pipe fitting could enter and then shrink to the rectangular channel size. As stated above, accurately creating rectangular slots of this size was a nearly impossible task to both program and execute using the CAM software and CNC machines. The final design incorporated the tapering into the chip assembly and expanded the width and length of the chip to allow for cylindrical shaped heaters to be centered at the channels.

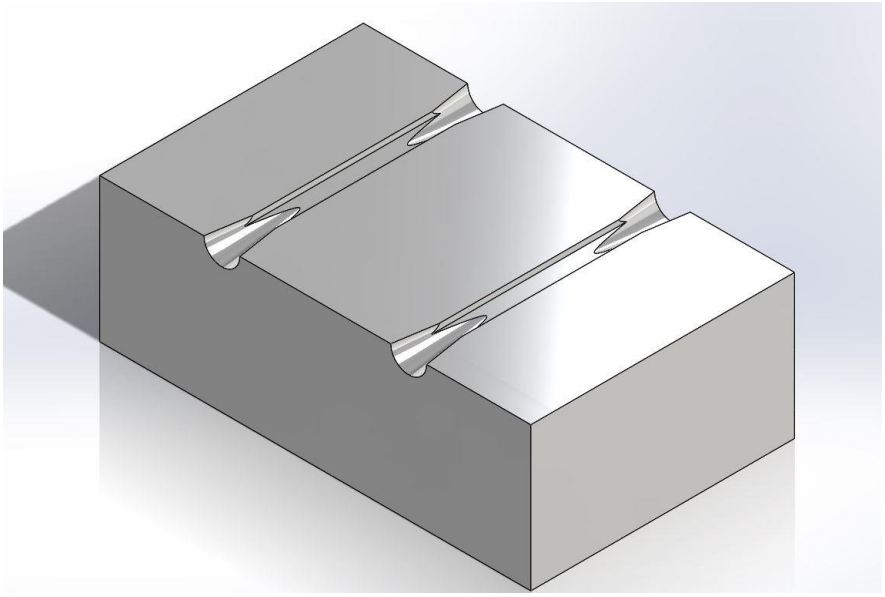

Figure 8: Final Teflon Micro-channel Chip Model.

Another major failure of the initial design iterations was with consideration to where heat sources would be attached to each channel within this compact assembly (i.e. considerations like wire connections, insulated heat transfer between channels). The heating sources needed to complete contact the fluid travelling in the channels and exclusively deliver heat in the individual

branches. The scale of channels and the necessity of precise dimensions exhausted traditional options like strip heaters and heat dissipation from resistors. Heater rods were incorporated into the final design.

Heater rods are cylindrical heaters that run current through resistors inside the sheath of the rods. The tips of the rods typically are not heated, but by insulated the sheath the conductive material, the heat would flow through the tips. Heater rods were incorporated into the final design by cutting inlets through the outside box's top piece which descend through the evaporator assembly and contact the center of the micro-channels. To isolate the heat generation completely through the tip of the heaters, a PTFE Teflon block was designed which completely surrounded the length of the heaters and fill the remaining cavity left between the chip and the box. The tips of the heaters rest upon rest atop the channels, effectively creating a 'lid' for the channels and the contact for heat transfer to the fluid. The chip was also made of PTFE Teflon so as to insulate the channels. Adding heater rods to the design affected the dimensions of the chip, where enough width was required to completely separate the heater rods.

The box enclosing the chips (the evaporator box) needed to, at this point in the design, seal the top chips together with minimal space around them, allow for both heater rods to come through the top, and can easily attach pipe fittings for connection to the entire loop. The final evaporator box was divided into two components, a top and bottom. The top component would have smoothly drilled holes centered where the heater rods would come down onto the channels of the chips. The bottom component has two threaded pipe fittings on either side that align with the entrances/exits of the channels. Both components had cavities, that when combined together, would compactly fit the chips together within them. These components both included long lips to bolt together and one piece includes an O-ring slot for a leak proof seal.

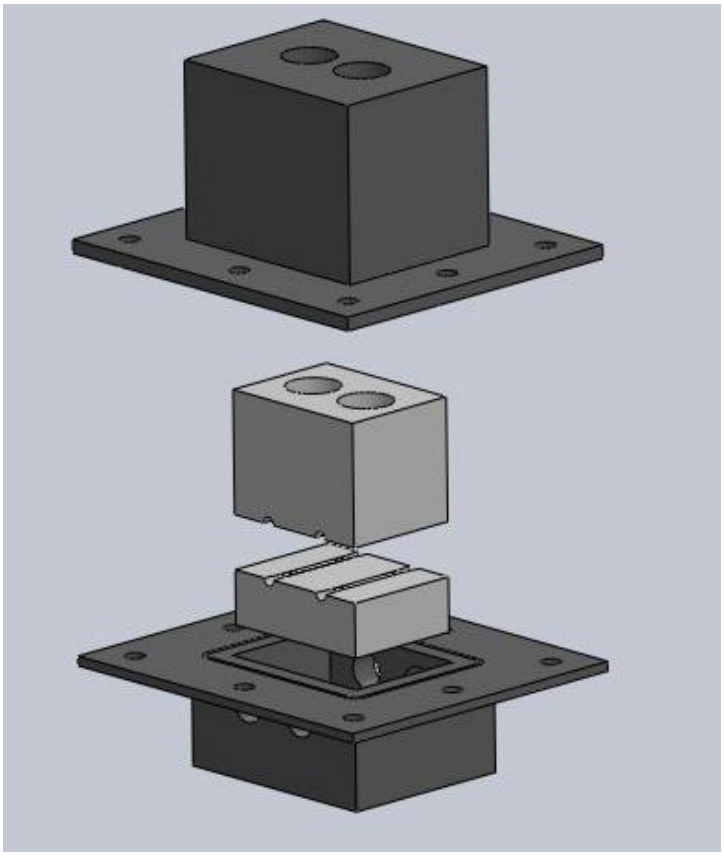

Figure 9: Final Evaporator Assembly Model.

2.3.3 Initial Calculations

Aside from initial background research on subject, as part of designing the loop, it was important to do initial calculations to understand the orders of magnitude which would be worked with. Many different types of calculations could be conducted, as this project touched on a wide variety of topics within mechanical engineering. Most notable calculations done involved using complex formulas to help with understanding ballpark figures, or served crucial to the design of the evaporator and the loop.

Conducting initial calculations are fairly important because they allow the project members to understand the magnitude of data which should be expected once experiments are conducted. Aside from doing calculations, previous reports with similar data could also be found and prove useful. Most of the calculations shown below were done using MATLAB, a technical computing language and software, and COMSOL, a Multiphysics modeling software.

Pressure Drop

One of the important calculations which had to be looked into for this project was pressure drop across the designed evaporator with the given parameters, as well the drop across the entire experimental loop. As an experiment which could be done in single phase, meaning there won't be much, if any, heat applied to the fluid R-123, allowing it to stay in liquid form. If enough heat would be applied, the R-123 would go from single phase to two phase, allowing more heat transfer to occur, but also causing additional variables and possible problems.

For single phase calculation for pressure drop, it was important to look at the Darcy-Weisbach equation, which relates the pressure loss due to friction along pipe and other sections of the experimental loop. The equation can be looked at either in pressure loss form or head loss

form. Head loss form would not be the right choice for this experiment because there is very little change in height for the fluid, meaning the equation below would be inaccurate to use [9].

$$Head\ Loss\ Form: \frac{\Delta h}{L} = f_D * \frac{1}{2g} * \frac{V^2}{D}$$

The equation used instead was the pressure loss form. This equation looks at the pressure loss due to viscous effects and similar to head loss, would be proportional to the length of the pipe. The equation used is shown below:

$$Pressure\ Loss\ Form: \frac{\Delta p}{L} = f_D * \frac{\rho}{2} * \frac{V^2}{D}$$

Where ρ is the density of the fluid in kg/m^3, L is the length of tube in m, D is the hydraulic diameter of the tube (either inner diameter if circular tube or another calculation for square or rectangular channels) in m, V is the flow velocity which is measured as the volumetric flow rate per unit cross-sectional area in m/s, and f_D is the Darcy Friction Factor [9].

For the experimental loop created for this experiment, the Darcy-Weisbach equation had to be used several times for different areas of the loop, assuming a constant inner diameter of the tube, while varying tube length, and then having a completely separate calculation for the evaporator, where parameters and shape changed. The total calculated pressure loss for the loop, would be as follows, assuming the same hydraulic diameter for all areas except the evaporator.

$$Evaporator\ Hydraulic\ Diameter: D_H = \frac{2ab}{a+b}\ where\ a\ and\ b\ are\ side\ lengths$$

$$\Delta p_{total} = \Delta p_{reservoirSect} + \Delta p_{mpumpSect} + \Delta p_{condenserSect} + \Delta p_{evaporatorSect} + \Delta p_{evaporator}$$

The sections were broken based on the different sections built and to allow for easy pipe length calculation. Overall, the only variety between each of the pressure loss terms are the lengths of the pipes and the hydraulic diameter for the evaporator. Another important variable required was the Darcy Friction Factor, f_D. The main two methods of finding the friction factor

was to use a specific formula, based on specific conditions such as laminar, turbulent, smooth pipes, etc, or using the Moody diagram as shown in the figure below [9]. In order to use any of the specific formulas, it was necessary to calculate the Reynolds Number (Re), and that same Re could be used in the Moody diagram to find the closest matching Darcy Friction Factor.

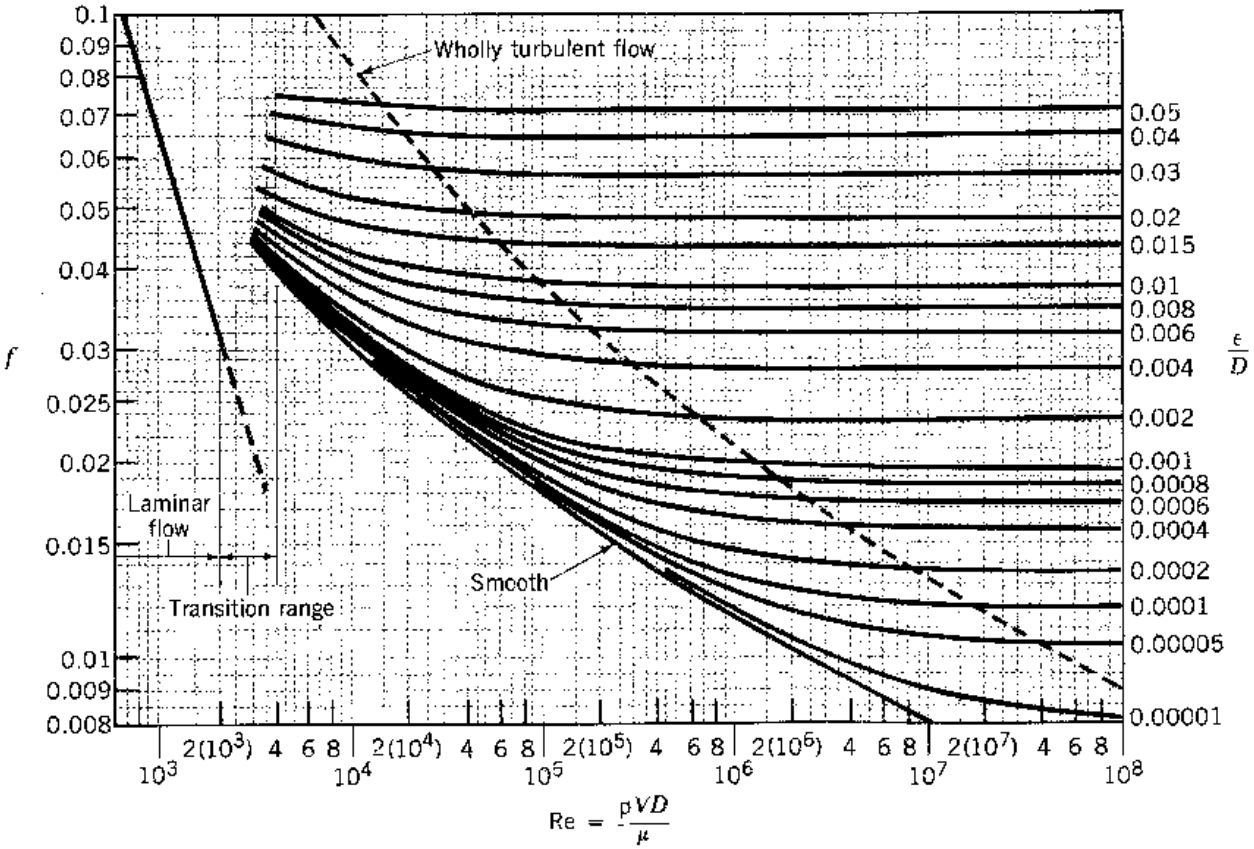

Figure 10: Moody diagram [9].

Formula for Reynolds Number and friction factor shown below as well:

$$Reynolds\ Number: Re = \frac{\rho V L}{\mu}$$

Where ρ is the density of the fluid in kg/m^3, L is the length of tube in m, V is the velocity based on the actual cross section area of the pipe in m/s, and μ is the dynamic viscosity in Ns/m^2.

$$Laminar\ Flow: f_D = \frac{64}{Re}\ for\ Re < 2{,}000$$

$$Turbulent\ Flow\ (Smooth\ Pipes): f_D = \frac{0.3164}{Re^{0.25}} for\ 4{,}000 < Re < 100{,}000$$

$$Turbulent\ Flow: f_D = \frac{0.25}{\left[\log\left(\frac{e}{3.7D} + \frac{5.74}{Re^{0.9}}\right)\right]^2}\ for\ 5{,}000 < Re < 3 * 10^8$$

In the pressure drop calculations, the values that varied usually were the velocity/flow rate, Reynolds Number, and the Darcy Friction Factor. This was because since flow rate would be an independent variable in this project, it wasn't justifiable to only do calculations for one velocity value. Also, as velocity varied, since proportional, Reynolds Number also changed, causing the friction factor to alter as well. The table below shows the values of pressure loss and flow rates at different sections, as well as the total pressure drop. To err on the side of caution, it was better to include a mechanical pump in the design in case the EHD pumps didn't perform to proper expectations.

Table 1: Pressure drop and flow rates through each section.

Velocity	Sect1P	Sect1FR	Sect2P	Sect2FR	Sect3P	Sect3FR	Sect4P	Sect4FR	Sect5P	Sect5FR	TotalP
[m/s]	[kPa]	[mL/min]	[kPa]	[mL/min]	[kPa]	[mL/min]	[kPa]	[mL/min]	[kPa]	[mL/min]	[kPa]
0.0001	0.000574	0.098504	0.000574	0.098504	0.000574	0.098504	0.000574	0.098504	0.006123	0.003462	0.008418
0.0005	0.00287	0.49252	0.00287	0.49252	0.00287	0.49252	0.00287	0.49252	0.030613	0.017311	0.042092
0.001	0.005739	0.985039	0.005739	0.985039	0.005739	0.985039	0.005739	0.985039	0.061227	0.034622	0.084184
0.0015	0.008609	1.477559	0.008609	1.477559	0.008609	1.477559	0.008609	1.477559	0.09184	0.051932	0.126276
0.002	0.018904	1.970079	0.011479	1.970079	0.011479	1.970079	0.020764	1.970079	0.122453	0.069243	0.185079
0.0025	0.027935	2.462598	0.014348	2.462598	0.014348	2.462598	0.030684	2.462598	0.153067	0.086554	0.240382
0.003	0.038433	2.955118	0.028356	2.955118	0.028356	2.955118	0.042216	2.955118	0.18368	0.103865	0.321041
0.0035	0.050335	3.447638	0.037136	3.447638	0.037136	3.447638	0.055288	3.447638	0.214293	0.121176	0.394189
0.004	0.063585	3.940157	0.046912	3.940157	0.046912	3.940157	0.069843	3.940157	0.244907	0.138487	0.472158

Evaporator Heat Transfer

Considering all the material options available and design constraints, it was important to simulate the heat transfer for one part of the experimental loop to make sure the heat would be directed in the proper intended section. After looking at all the variety of software available, it was decided that COMSOL would be the most beneficial. A design which was added to the

evaporator assembly was polytetrafluoroethylene (PTFE) casing around the evaporator heaters. This was a crucial addition because looking at the design of the heater, shown in the figure below, heat would escape from the sides and the bottom. This was less than ideal for the project because the project required the heat to just be applied to the bottom, meaning the two parallel, small channels representing the microelectronic chip.

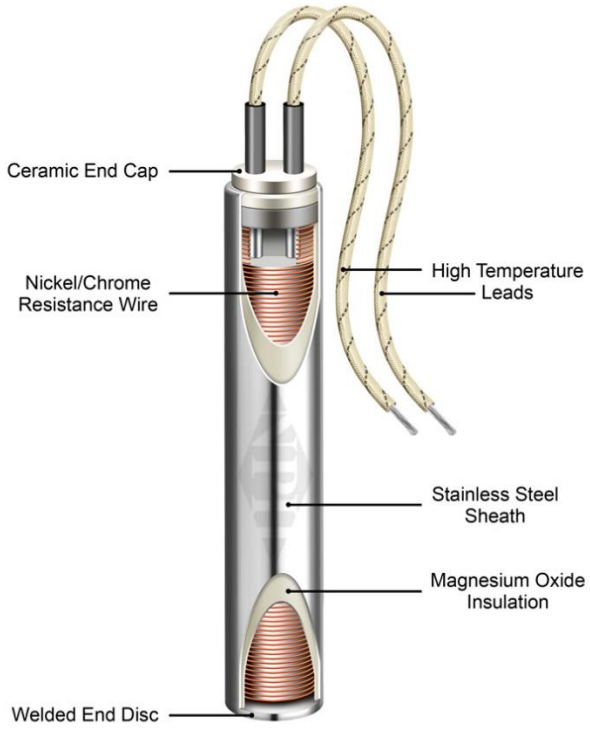

Figure 11: Hi-Density Cartridge Heater (Omega).

Given the properties of PTFE, this material seemed like the best option for making a casing for the evaporator cartridge heaters. Some of the benefits of PTFE are high heat resistance, meaning it can operate continuously at high temperatures, very low thermal conductivity so heat will be well contained within the sides of the evaporator heaters as long as the design meets the standards. Another huge benefit of PTFE is that it offers high dielectric strength while being completely resistant to almost all chemicals [10].

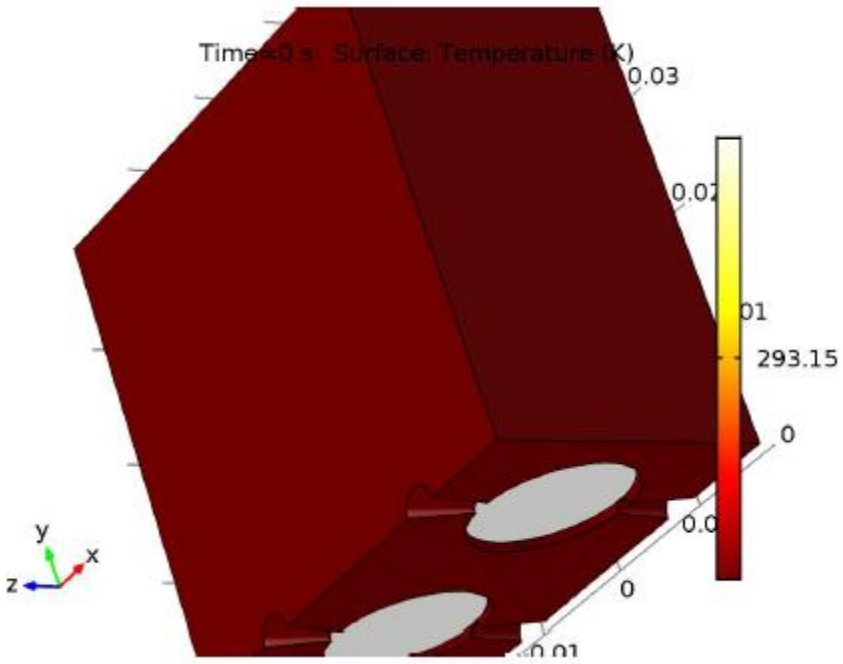

Figure 12: Evaporator - Conduction heat transfer.

Using COMSOL's conduction heat modeling software, after inputting in SolidWorks files, and observing the heat distribution as shown in the figure above and by looking at the properties of PTFE, it was easily concluded that this material would provide a good insulation and force the heat generated by the heaters to leave from the bottom and right into the parallel channels.

Condenser Length

Another important calculation which had to be conducted was figuring out the length required for the condenser. The condenser is the location where after the fluid has been heated and possibly turned into two phase, ideally almost all vapor, phase changes back to all liquid as it travels through an ice water bath. Basically, it was important to note that the amount of heat added in the evaporator would determine the amount of heat which must be removed in the condenser, and since the fluid would travel at a constant rate, the length would definitely play an important role.

Using knowledge from heat transfer, it was recognized that the heat added and absorbed by R-123 was given from the equation below:

$$Q_{Evaporator} = Q_{Vaporization} = mh_{fg}$$

$$m = \rho V = mass = density * total\ volume\ of\ 2\ channels\ in\ evaporator\ [kg]$$

$$h_{fg} = heat\ (enthalpy)\ of\ vaporization\ \left[\frac{J}{kg}\right]$$

Since the mass was not given and much harder to measure, the easiest way was to substitute that variable for the product of density and volume. Looking at the overall design and logic behind the condenser, an equation for the heat loss was derived:

$$Q_{Condenser} = \frac{T_1 - T_2}{R_{conv,1} + R_{cond} + R_{conv,2}}$$

The three resistances values represent the convection of R123 within the tube, the conduction of R123 from the tube to the ice bath, and the convection to the environment, respectively. In the end, it was determined that the first resistance value was very complex and was really only required for two-phase experimentation, and thus was assumed to be nonexistent. The resistance equations for all three are shown below:

Convection of R123:

$$R_{conv,1} = \frac{1}{h_1 A_1}$$

$$h_1 = h_f * \left[(1-x)^{0.8} + \frac{3.8 * x^{0.76} * (1-x)^{0.04}}{p^{0.38}}\right]$$

$$= 0.023 * Re^{0.8} * Pr^{0.4} * \frac{\lambda}{D} * \left[(1-x)^{0.8} + \frac{3.8 * x^{0.76} * (1-x)^{0.04}}{p^{0.38}}\right]$$

$$A_1 = 2\pi r_1 L$$

Convection of environment:

$$R_{conv,2} = \frac{1}{h_2 A_2}$$

$$h_2 = h_f * \left[(1-x)^{0.8} + \frac{3.8 * x^{0.76} * (1-x)^{0.04}}{p^{0.38}}\right]$$

$$= 0.023 * Re^{0.8} * Pr^{0.4} * \frac{\lambda}{D} * \left[(1-x)^{0.8} + \frac{3.8 * x^{0.76} * (1-x)^{0.04}}{p^{0.38}}\right]$$

$$A_2 = 2\pi r_2 L$$

Conduction of R123:

$$R_{cond} = \frac{1}{2\pi kL} \ln\left(\frac{r_2}{r_1}\right)$$

Since one resistance value was omitted, it was important to keep a safety factor in mind and a value of 3 was chosen. Using MATLAB to do the calculations and comparing the heat values of the evaporator and condenser, the length was produced and shown in the table below, dependent on what the temperature inside the condenser (ice bath) would be. Looking at the table, it can be concluded that as the temperature of the condenser dropped, the length also dropped proportionally since more heat transfer would occur due to the difference in temperature.

Table 2: Temperature of Condenser vs. Length.

Temperature of Condenser (^{o}C)	**Condenser Length (in)**
-10	2.31
0	3.14
5	3.83
10	4.90
15	6.81

From the table shown above, it was concluded that, even with a safety factor, utilizing a plastic box as a condenser with temperature going as high as 15 degrees to cool down the R-123 was still more than enough, as long as the box was longer than 6.81 inches.

2.4 Evaporator Manufacturing

Once the design calculations pertaining to the evaporator were completed and computer-aided models were generated of the four components of the assembly, the manufacturing of each of the evaporator pieces was undertaken. The outer pieces of the evaporator assembly housing were machined from type 304 stainless steel, which was purchased by the team from Speedy Metals. The inner pieces of the assembly which form the evaporator micro-channels were machined from Teflon purchased from Ultimate Plastics. With the assistance of Nova Biomedical machinist Dave Richard, computer-aided machining (CAM) models of the stainless steel components and the top half of the Teflon micro-channel subassembly were programmed using the software MasterCAM. In order to be exposed to the variations between programs, CAMWorks software was utilized for the programming of the bottom half of the Teflon micro-channel subassembly under the guidance of Nova Biomedical machinist Andrew Barakos.

During the generation of the CAM models extra attention was paid to the non-critical design dimensions, particularly for the stainless steel pieces, in order to make reductions to machining time. Due to the hardness of type 304 stainless steel it was necessary to make much slower, higher interval cuts than though performed in machining the Teflon. All evaporator assembly pieces were machined using Haas MINIMILLs, the run-time on which was between five and seven minutes for each of the Teflon parts and between four and a half and five and a half hours for each stainless steel piece.

Special care was taken to clean and deburr all evaporator components in order to ensure that no debris would be swept into the fluid flow once the loop was assembled. The branch inlet holes on both sides the bottom half of the outer evaporator shell were carefully taped by hand so

as to confirm that the threading of the connecting nipples would come flush against the surface of the Teflon chip and create the smooth possible flow transition for the working fluid.

2.5 Experimental Loop Assembly

After initially learning about the topic and doing research, designing and redesigning, and doing important calculations, it was finally time to put the different components of the experimental loop together.

This process of the project started definitely past the timeline and that is because the group had many setbacks and problems. Aside from problems with the design and manufacturing, causing ideas to be scrapped and reworked, assembly was a whole another issue. Initially, the main concern was the resources available in the lab. While this project was being designed and worked on, there were at least three other projects going on concurrently, causing the resources to be spread very thin. Due to the nature of the project and experiment, while some parts could be purchased even though high cost, others were too expensive to have multiple of in the lab.

One of the experiments running in the lab was especially important because it contained a lot of the necessary components of the project loop, and delays with that project caused further delays with this project. The first thing grabbed from the ended experiment was the platform. In order for this project to get to assembly phase, it was important to have a platform on which components could be added. Unfortunately, since the design was based around the evaporator, the evaporator side of the loop was a little longer than expected and required the team to add additional support and make an even larger platform. Once the platform was built, parts had to be laid out so then holes could be drilled for areas with the differential pressure transducers, as well as a place for the reservoir.

Overall, the assembly was an accomplishment and was completed in a week or so and the loop looked very well made. As shown from the top overview figure, the loop assembly was successful but the holes and drilling from the old experiment looked a little unorganized. This section of the report will go through the different sections of the loop, with assembly work and challenges discussed.

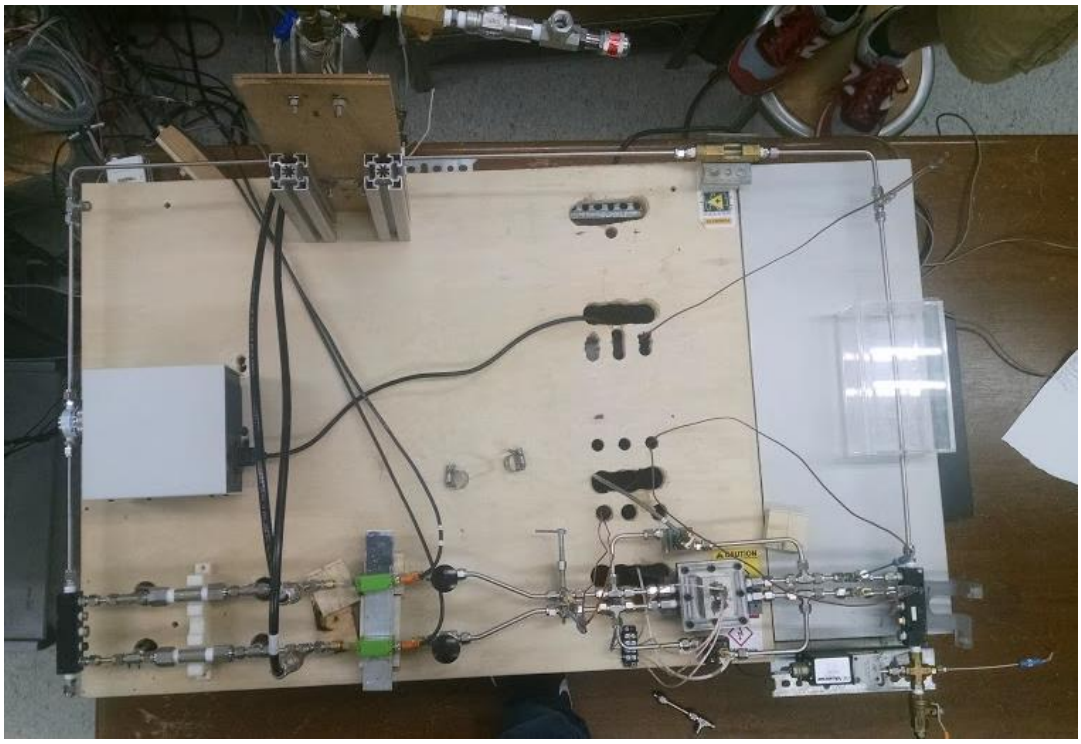

Figure 13: Top overview of the experimental setup.

2.5.1 Evaporator

Being the longest and the most time consuming part of the assembly, the evaporator side of the loop was the length defining side, which determined the lengths of the other sides of the loop. Even though it was very time consuming, this side was also the most important section of the experiment so it had to be accomplished in an extremely careful manner.

Before the previous experiment was completed, one of the tasks the team completed was to go through each side of the experimental setup and scrounge around the lab to find required

and additional parts, fittings, etc. Going through each connection and fitting was very tedious, and since this had to be done before actually assembling, there was always worry that parts had been forgotten. Thankfully, ordering parts didn't take very long because, aside from getting approval from the lab manager or supervisor, most of the vendors who sold these parts guaranteed next day arrival at a very low shipping expense.

Figure 14: Differential pressure transducers configuration.

Because the lab was spread thin on resources such as crosses, this side of the loop had a lot of T-fittings, which ended up increasing the length of the side. It was important to be sure that each component of this side had been accounted for, because any missing pieces could have proved fatal. Fortunately, with careful planning, there was enough space for the first two differential pressure transducers in parallel channels to be hanging below the experimental setup as shown in the figure below. EHD pumps being the most important aspect of the experimental setup, it was crucial that the pumps being used, same as the ones from the old experiment, still worked and had a high performance.

Prepping the EHD Pump

Before the EHD pumps could be added into the project experimental setup, proper care and prepping was required. Since the pumps were used in the previous year-long experiment, the pump had a lot of contamination, and just being unclean. To make sure this would not cause an issue, the pump was soaked in an isopropanol bath overnight to remove any remnants of R-123 and other material, while also deep cleaning the tiny channel shown in the figure below, for the EHD pump, through which the fluid would move.

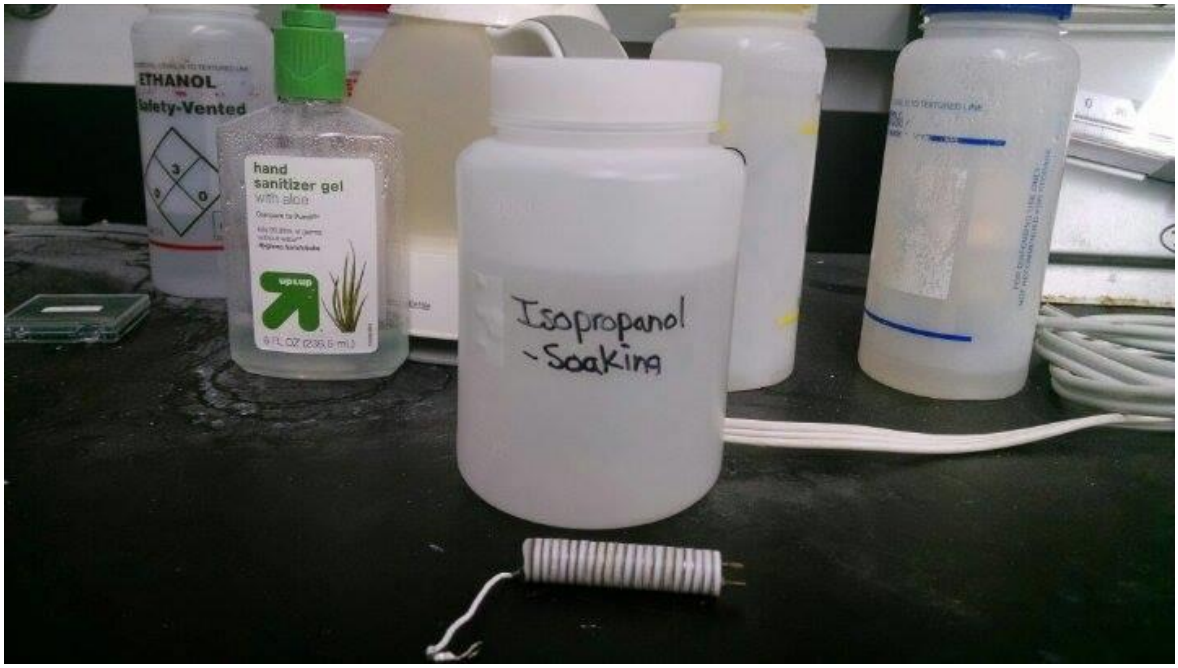

Figure 15: Cleaning of the EHD Pumps.

After cleaning, it was very important to next check the performance of the EHD pump and observe whether components of the pump had degraded, since some data from the past experiment pointed towards performance issues. The simple solution which was implemented was to check each electrode of the EHD pump, by running current through each electrode in the power line to check and see whether the corresponding electrodes were attached and working. This was accomplished using a multimeter and is shown in the figure below. By doing this

simple test, the group was able to conclude that out of the three equal pumps available, only two passed the performance inspection.

Figure 16: Checking connection of electrodes to bus lines.

Powering the EHD Pump

Once the checks were complete, it was finally time to move on to the next step of adding the EHD pumps to the experimental setup. This was a very sensitive process because the EHD pumps had to be attached to the power wire through once side, while being grounded and having another wire soldered to a stainless steel fitting on the other side.

The wiring of the voltage sources for the EHD pumps, which utilized high voltage feedthroughs to, required some additional thinking because there had to be a feedthrough, which only connected to a national pipe thread taper (NPT), which then had to connect to a yor-lok compression fitting to then connect to a corresponding T, allowing it to be a part of the experimental setup. The fittings also had to initially be large enough to incorporate the high voltage feedthrough, but also be a tight enough fit so that there was no leak and R-123 would

have no way of entering. Shown below in the figure is what the group came up with based on what was available in the lab, and though it looked strange, what really mattered was that it worked flawlessly.

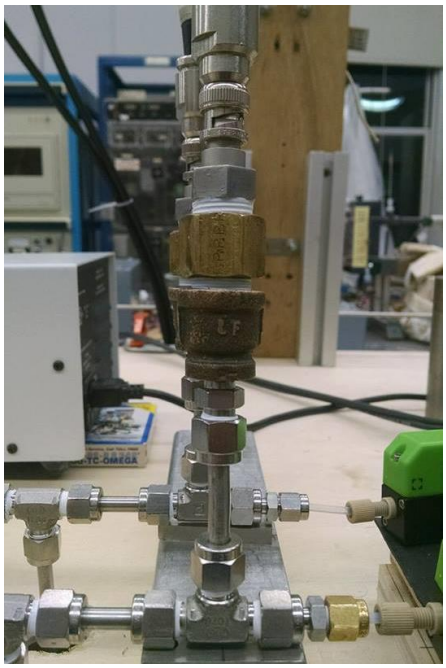

Figure 17: High voltage feedthroughs.

Once the power section was attached to the loop, while having a wire go through each of the different fittings and connections to get to the point of the EHD pump, the EHD pump could finally be attached. Keeping length in mind, the negative/ground side of the EHD pump had a small wire attached which was soldered to the stainless steel fitting. This was a very painstaking process because solder generally does not want to stick to stainless steel. As a result, thermal heat flux paste had to be applied to the stainless steel area, followed by using plenty of solder and letting it flow between the wire and the steel location. Heating up the area took a very long time and there were many times when the connection was not strong enough and had to be redone. Finally after the connection was secure, the thermal paste had to be cleaned and scrubbed

because it had a tendency of affecting the performance of the EHD pump and causing the resistance of the setup to decrease tremendously, not to mention cause contamination.

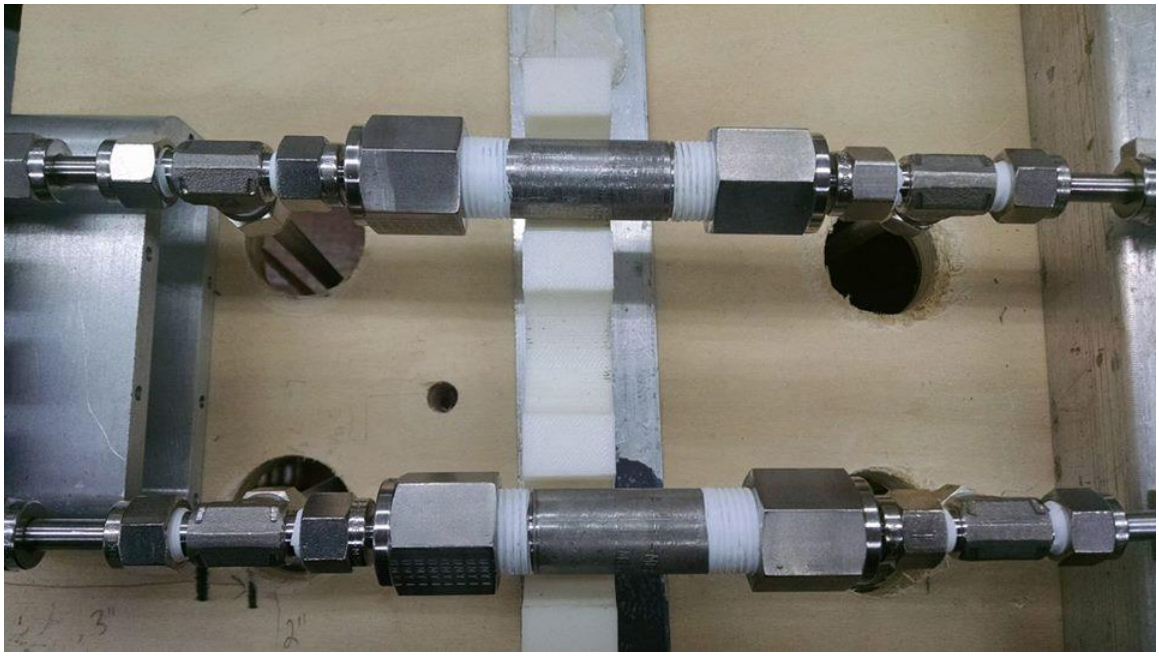

Figure 18: Complete assembly of the EHD pumps.

Before the EHD pump was inserted into the pipe nipple, it was cleaned once again with isopropanol and wrapped in Teflon tape to allow for a clean and much tighter fit. Finally, the wire from the high voltage feedthroughs were soldered to the positive/power side of the EHD pumps and the connection was complete. The completed EHD assembly looked like the figure below, with many components such as wire, solder, and Teflon tape inside, which couldn't be seen.

Prepping for the Evaporator

After the addition of the flowmeters, which will be discussed later in the sensors section, valves were added so then additional experiments could be conducted. Advantages of the valves are that they allow single branches to be run at a time, but also allow maldistribution experiments to be performed. In order to prep for the evaporator coming up, the first thing which had to be

addressed was the distance between the two branches. Initially, the distance was great to allow for the sensors and power to fit without rubbing against each other and being an issue. To have a smooth transition, and have the branches fit perfectly in the evaporator, tubes had to be bent at an angle which was not overly steep, while keeping the bent tube at a reasonable length. Using simple trigonometry, an optimal length and angle was calculated and the pieces were bent using a manual tube bender available in the lab. The result and the tool are shown in the figure below.

Figure 19: Manual tube bender.

After the bent pipe decreased the distance between the two branches, thermocouple probes were added, along with additional set of differential pressure transducers for each branch. A couple fittings were also included to create a great transition from tube yor-lok compression fittings, to NPT, and finally into the complex evaporator.

Manifolds

On either end of the evaporator side was a manifold to allow for easy connection of the branches, especially due to the change in distance between the branches. This also allowed for

additional connects at the end of the loop, as shown in the figure below, and allowed to loop to continue to the condenser and mechanical pump side with a smooth transition. This method was proved to work successfully because it had been done previously in experiments with positive results.

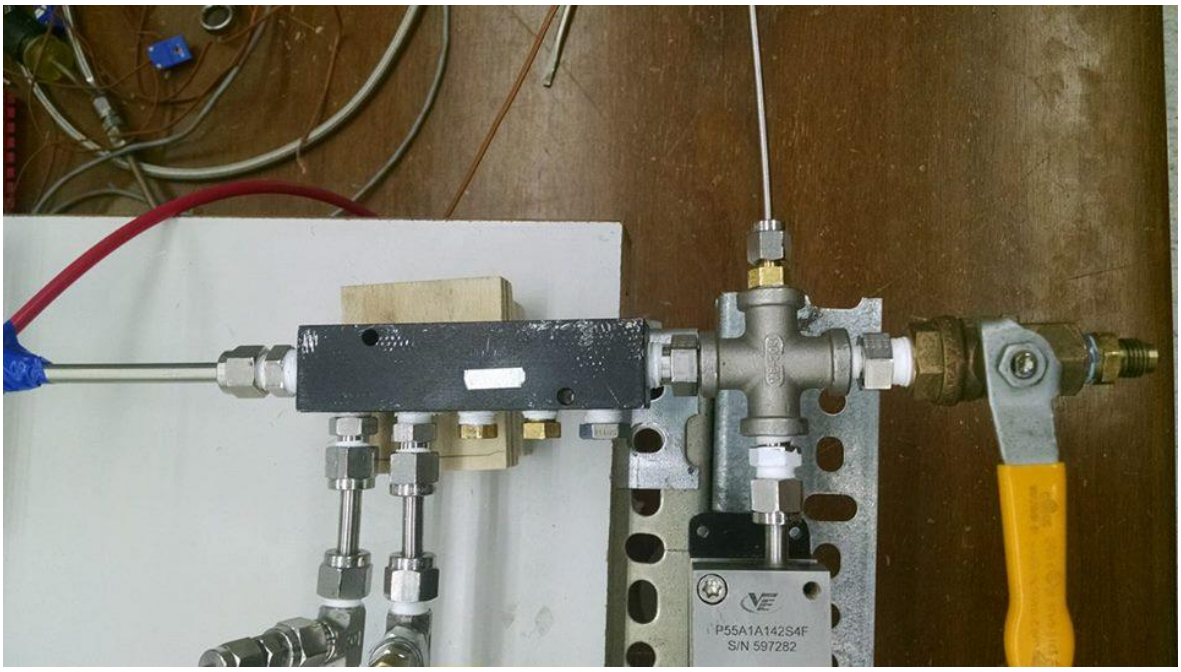

Figure 20: Manifold attached to the evaporator section.

In the manifold at the beginning, there was a connection which was used during leak testing, but otherwise there was just a pressure cap in case another port or valve was ever required. In the manifold near the end of the evaporator section, a cross fitting was added. Here, the important absolute pressure transducer was attached, along with a thermocouple probe, and finally a valve to allow for leak testing as well as give the ability to pull a vacuum in the experimental setup. Both of these important topics will be discussed at greater length at a later point in this report.

2.5.2 Condenser

Another important side of the experimental loop was the condenser section, which would have to include the condenser itself and a thermocouple probe. The condenser length was calculated during the initial calculation section to be around 3 to 4 inches. Given that the previous experiment already had a condenser with a length of 6 inches, it was more convenient to utilize the same part and make it work with the setup for this project. Aside from removing brass pieces and adding stainless steel tube and compression fittings, the rest was kept the same. The length of the condenser side was estimated based on where it made sense to put the reservoir, and based on the length of pipes available, since creating new tube bends and adding sleeves and nuts would be very expensive and time consuming process. Figure below shows this section of the experimental setup.

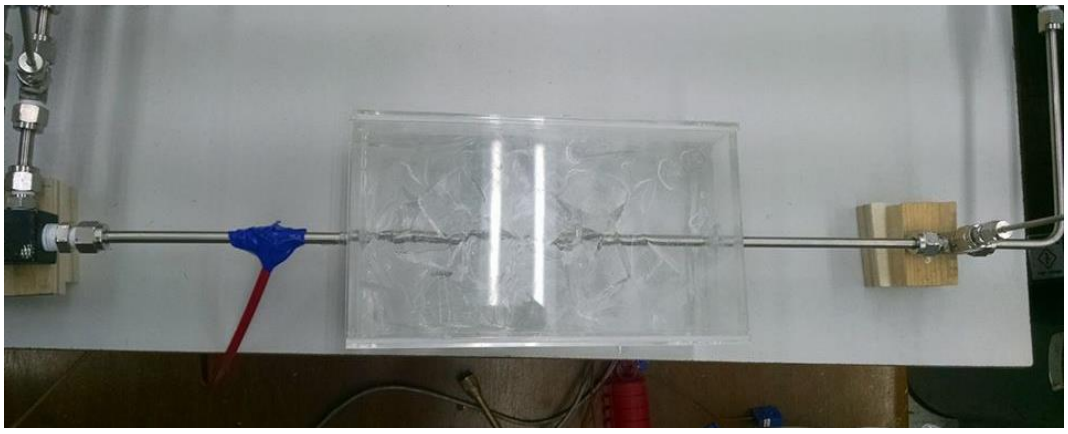

Figure 21: Condenser section.

2.5.3 Mechanical Pump

The next important side of the experimental loop looked at was the mechanical pump section, which was extremely simple because it only needed two correctly measured pieces of tubes with a T-fitting in between and a good bend to arrive at the reservoir inlet. The T-fitting was included in case another absolute pressure transducer was ever required, especially when

doing two-phase experiments or for an additional temperature reading. Aside from a little height bend/difference which occurred due to the outlet fittings for the mechanical pump, the rest of the side looked fairly simple to assemble. Figure below shows this section of the experimental setup.

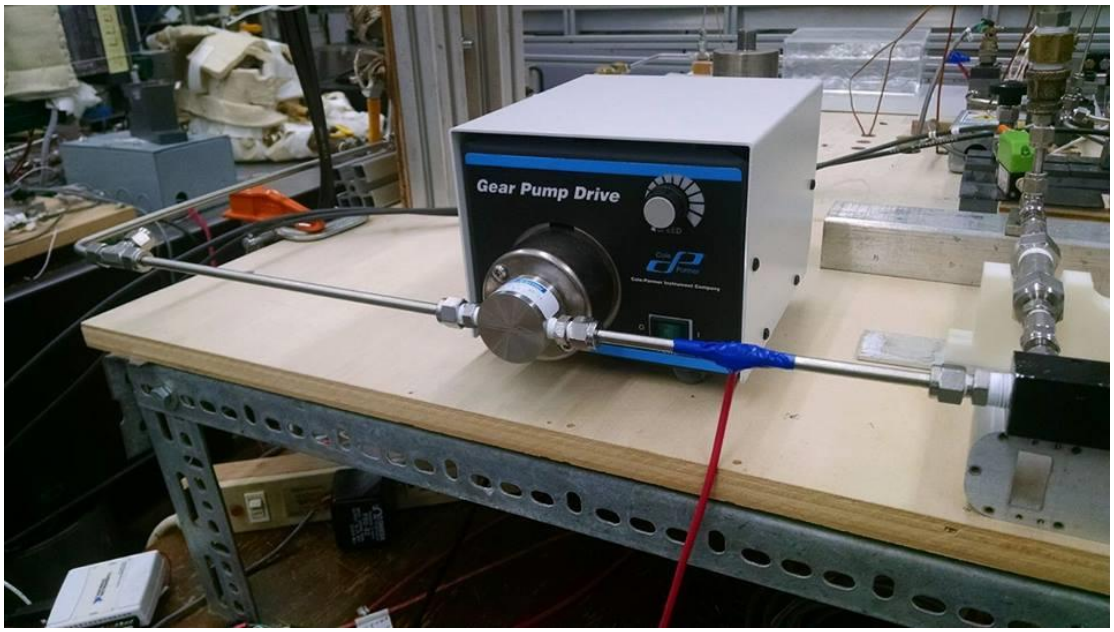

Figure 22: Mechanical pump section.

2.5.4 Reservoir

The final side of the experimental loop, which was extremely important was the reservoir section. Even though there were not a lot piece involved, it was crucial to make sure that the length of the reservoir side equaled the length of the evaporator side. This was one the main reasons that this side of the loop was saved until the last minute. The reservoir itself was taken from the previous experiment since that was a largest unused reservoir available and could be used to fill the experimental setup for this project. Also, even though there were a lot of brass pieces, the reservoir had already been through leak testing countless times so that would be one less problem to deal with. The reservoir section also contained a copper see-through section,

which would allow the group to check and see if bubbles formed or if vapor was going inside the reservoir. Figure below shows this section of the experimental setup.

Figure 23: Reservoir section.

2.6 Sensors Configuration and Calibration

An experimental setup used in this experiment required many different types of sensors. In order to gather useful data, it was important to have information such as pressure difference between the two EHD pumps as well as the pressure drop within the evaporator for each of the separate branches. It was also crucial to have knowledge about the flow rates in each of the branches since that would determine the performance of the pump. Finally, it was also important

to have temperature readings at various locations, especially to see how the temperature varied after the evaporator and after the condenser.

2.6.1 Flowmeters

An important and expensive addition to the project's experimental loop was the flowmeters. These are very expensive flowmeters produced by a company named Sensirion and they are specifically tailored towards flow control systems requiring high precision due to low flow rates. These flowmeters were added to the evaporator section of the loop, one for each branch. There was a little bit of planning required again to have a smooth transition for these flowmeters because they only accept plastic tubing of size 1/8 inch. Thankfully, since the ones connected already had these plastic tubes with sleeves and compression fitting nuts, it was simple to find a 1/8 inch to 1/4 inch adapter. Shown below is a figure of the flowmeter described above.

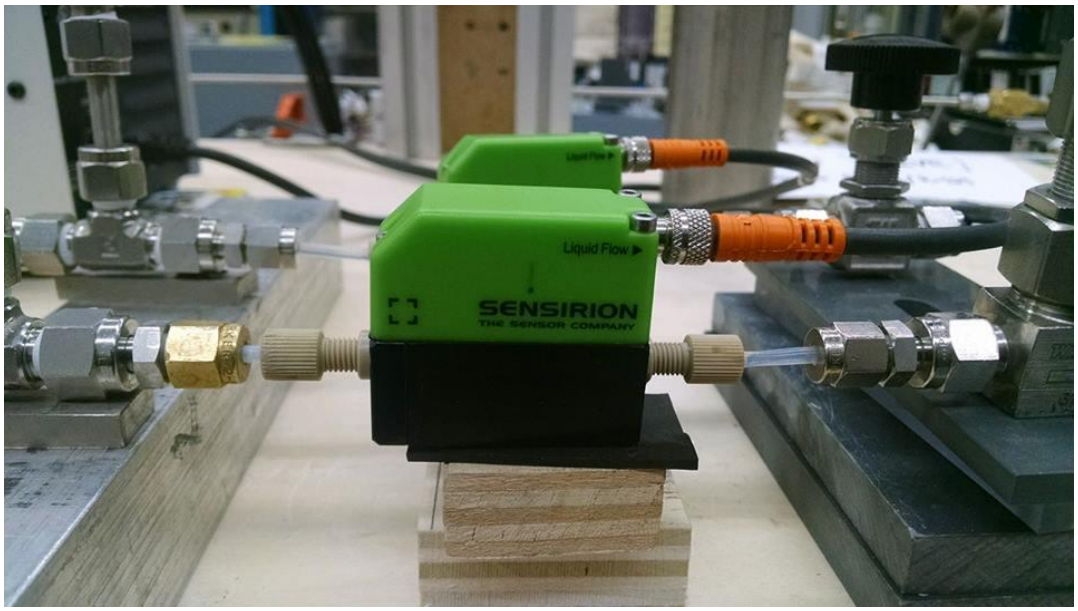

Figure 24: Sensirion flowmeters.

These flowmeters were a major source of leak because the length of the tubes weren't initially taken into account while building the loop. Also, since plastic tubing was used, it tends to be extra flexible and the plastic sleeves which went inside the flowmeters kept coming out because they weren't properly attached. These sleeves and the lengths of the plastic tubing had to be constantly adjusted and finally, to make sure the sleeves never came off for a while, Teflon tape was used as a small amount to allow for a strong connection and less chances of a leak.

Calibration for these sensors were conducted by putting each of the flowmeters in series and gathering points to see voltage output versus actual flowrate. Fortunately, since these sensors are extremely expensive and very sensitive, the lab monitor, Lei Yang, carried out the calibration for the group and just provided the groups with the calibration curves like the one shown below in figure. This information was then inputted into LabVIEW so when the program was run, the correct data could actually be produced. Looking at the raw data, the information in the y axis was flowrate in milliliter/minute and the information in the x axis was the voltage outputted, but to include another problem with calibration, the given data had to be subtracted by five.

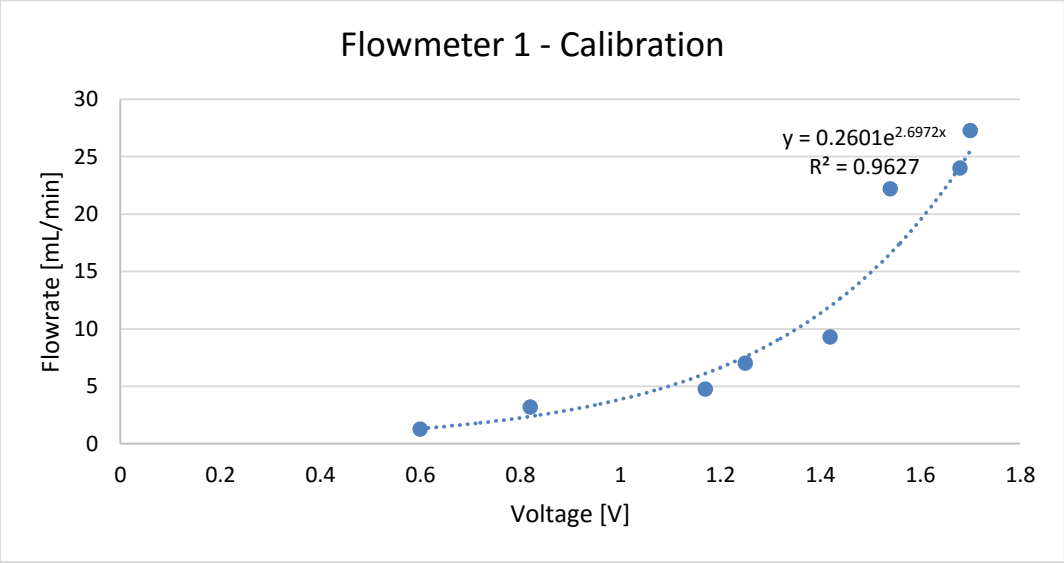

Figure 25: Calibration of Flowmeter 1.

2.6.2 Differential Pressure Transducers

Another required addition to the project's experimental loop was the differential pressure transducers. These sensors are produced by Validyne Engineering these sensors are able to thrive in a wide range of pressure measurements, from 2.22 inches of water column to almost 3200 psi [12]. The only change was that to get a specific range of pressure measurements, it was important to switch the diaphragms, which determine the sensitivity and range of the differential pressure transducers [12]. For this project, the diaphragms used were number twenty two for each of the four differential pressure transducers because that diaphragm range and sensitivity was known to work at this scale and was used in the past experiment.

Figure 26: Differential pressure transducer calibration apparatus.

Before using each of the sensors, they had to be prepped for calibration, meaning deep cleaning had to be done. Using isopropanol and DUREX non-woven polyester, each of the differential pressure transducers were opened and wiped down, with each O-ring also wiped clean, until the color change on the non-woven polyester had minimal change. Once cleaned, each sensor was ready to be calibrated using the apparatus shown above in figure, along with red manometer oil to mark the change in pressure, and National Instruments Max to observe corresponding voltage. During calibration, it was also important to note that the span had to be at least of five volts or higher, and these values for range and zero point could be adjusted, using the demodulator to which each differential pressure transducer was attached to. The figure below shows the calibration curve of one of the differential pressure transducers which showed the relationship between pressure and voltage.

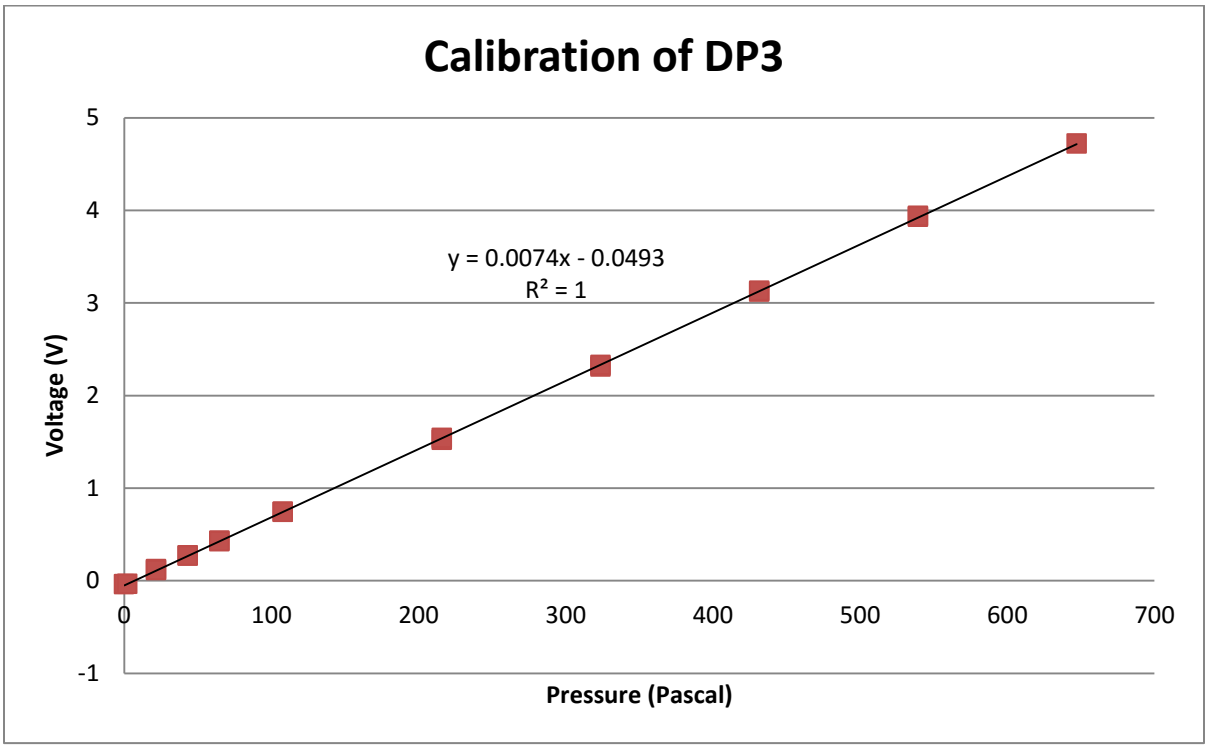

Figure 27: Calibration of a Differential Pressure Transducer.

Something important to note is that this calibration had to be done multiple times in order to achieve a very high coefficient of determination (r-squared) value, at least 0.999. The calibration apparatus used measured pressure in water column but used oil so the independent variable, pressure, had to be converted from inches in oil column to pascal. Since these were all linear relationships, aside from changing the intercept and slope of the equation slightly, the most important r-squared value remained unchanged.

2.6.3 Absolute Pressure Transducer

Absolute pressure transducer was another sensor required for the experimental setup. Absolute pressure is referred to the vacuum of free space, meaning there is zero pressure [13]. In this project's loop, this sensor's responsibilities were to measure atmospheric pressure and ensure that there was a fixed vacuum pressure applied within the loop, once a vacuum was pulled [13]. In terms of calibration, since the same sensor and demodulator were being used, the calibration data used by the previous experiment was utilized again.

2.6.4 Thermocouple Probes

Thermocouple probes are sensors used for measuring temperature at specific locations within the experimental setup and they are essential especially for two-phase experimentation. Even though this project might not go into two-phase experiments, the setup was created and designed in a way to have two-phase capabilities. The table below shows the strategic positions of each of the thermocouple probes.

Table 3: Locations of the Thermocouple Probes.

Thermocouple Probe	Location
1	Branch 1 – Inlet
2	Branch 2 – Inlet
3	Branch 1 – Outlet
4	Branch 2 – Outlet
5	Near Absolute Pressure Sensor
6	Condenser – Outlet
7	Reservoir

2.7 Data Acquisition

In order to gather all the data being outputted by the sensors, data acquisition boards were required, especially those that could measure electrical and physical phenomenon such as voltage, current, and temperature. These DAQ boards are all connected to the computer, allowing these values being recorded, to be converted into something useful and usable. Each DAQ board has around fifteen analog input ports and some have a couple analog output ports to allow the user to send inputs to voltage sources.

2.7.1 Electrical and Grounding

The electrical configuration of each of the sensors required some designing and understanding where each wire was and should be connected. While the previous experiment setup was still being used, an extensive map was drawn out for where each of the connections went to, whether into the DAQ board as analog input, power supply, ground, or into a thermocouple input. Refer to the appendices for different tables which correspond to the variety of sensors and which DAQ board and analog input channel that each sensor connected to. Shown below in the figure is an example of one of the data acquisition boards which has inputs for the differential pressure transducers, and the voltage and current source for the EHD pumps.

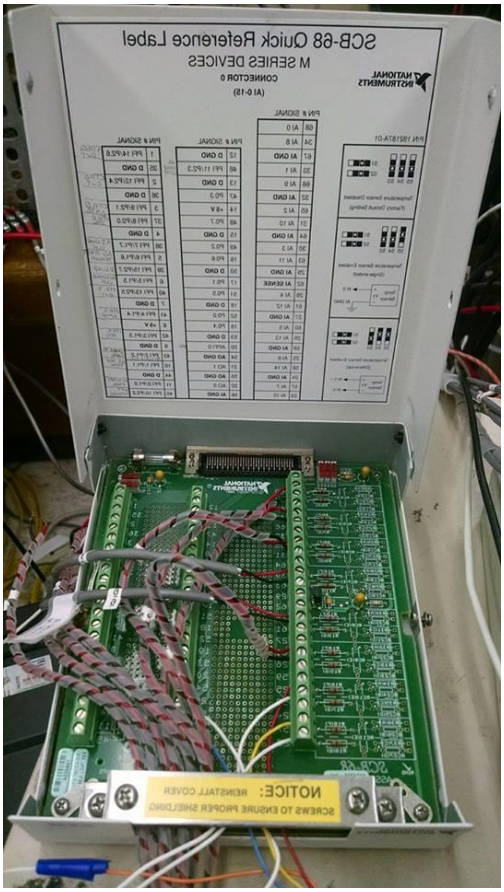

Figure 28: DAQ Board.

In order to make sure that the experimental loop was grounded, it was crucial to check whether the entire loop was connected or not. This was accomplished through the use of a multimeter, using the control function. While touching one electrode at one point of the loop, the other electrode was moved around and touched many different locations of the loop as shown in the figure below. If there was conductivity, meaning the loop was connected, the multimeter beeped, which concluded to only having to use one grounding wire for that section of the loop. To the group's amazement, the entire experimental loop was connected and technically, only one grounding wire was required. To be safe, a ground was added next to the condenser, and then another was added on the opposite side, next to the mechanical pump.

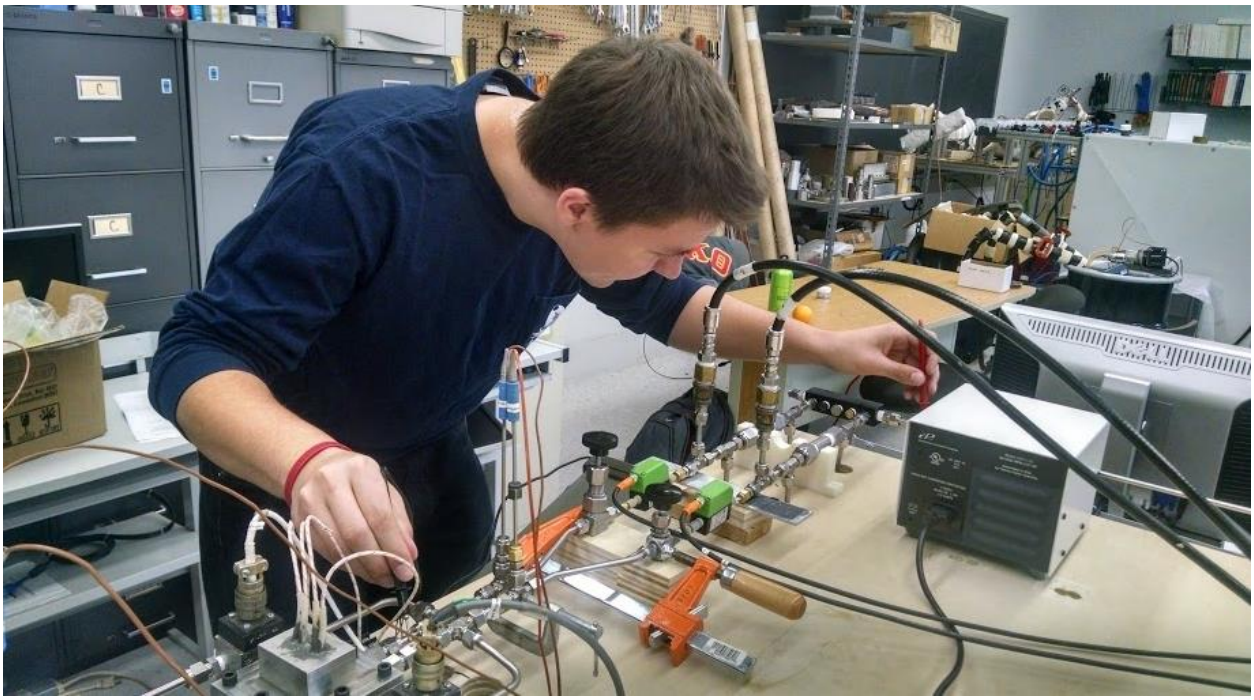

Figure 29: Conductivity testing for grounding.

2.7.2 LabVIEW

In order to gather data from all of the sensors, process it to be understandable and usable, LabVIEW software was deemed most user friendly for the task at hand. Having a graphical programming interface, the project group was easily able to create and edit previous programs to be compatible with the current experimental setup. Some simple changes had to be made such as the channel locations for each of the sensors, and the calibration equations for differential pressure transducers and flowmeters. Three major changes had to be made to LabVIEW in order to make the program usable for experimentation; creating a safety feature/emergency shutoff, getting all data written into an excel file, and organizing of the user interface.

The previous program attempted to create a safety feature but it didn't end up working the way it was intended to. The experiments being conducted could be very dangerous and so it was important to have a shutdown for two cases; if the current or the voltage being inputted by the EHD pumps exceeded a certain constant value. Over these values, the pump would start

cracking and cause sparks due to the fluid violently ionizing. Even though having a “Stop Program” button was helpful, even that split second human error could prove to be catastrophic and as a result, the computer was programmed to handle it. After a few attempts, the program was fixed to supply zero voltage to the pumps and shutdown as soon as any of the constraints exceeded the maximum values.

Another important change was the removal of writing data to the text file and introducing the gathering of data into an excel file, making it accessible for creating graphs and tables, and definitely in a better format over a text file. The base code was already written during a course at Worcester Polytechnic Institute which involved LabVIEW, and so implementing that section to work with the group’s code wasn’t too complicated. Finally, it was beneficial to make adjustments to the user interface created by LabVIEW so that during experimentation, the output data would be organized, easy to follow, and visually appealing.

2.8 Experimental Preparation

Before experiments could be conducted, major steps had to be taken to ensure proper preparation and safety of the experimental setup. These steps had to be completed carefully since they would definitely alter the results attained from the experiments.

2.8.1 Leak Testing

Leak occurred in the experimental setup when connections were loose, pipes had a bend, or a change in material was implemented. In order to do a leak test, a flare fitting and pressure line inlet was connected to the valve in the experimental loop and the high pressure line was pressurized to approximately twenty psi. Before the pressure line connection was inserted into the assembly, a pressure gage was attached to the other side of the loop, next to the branch inlet

manifold, which could read whether pressure was being lost after closing the valve. The experimental setup was then pressurized to ten psi, and then the once the valve was closed, the leak rate measurement commenced.

2.8.2 Methods of Leak Testing

After initially pressurizing the setup, the air was leaking out of the loop almost immediately, confirming that there was an enormous leak problem due to connections not being tightening properly. A common method of leak testing was to pressure the setup, and then slowly check each connection by adding bubbles created by soap and water. If a leak was big enough, the bubbles grew due to the air leaking out.

A more uncommon method of leak testing involved putting an entire section of the loop underwater, making sure nothing electrical was included, to check for bubble formations and locations. The group had to utilize this approach to observe whether the viewport, which was copper, was leaking or not. Shown in the figure below, this method was actually very successful and there was enough reason to remove the viewport currently attached and find a few one.

Figure 30: Underwater leak testing method.

Once the soap bubbles stopped proving to be useful, the final course of action was to take apart the entire loop and check leak section by section. The main goal was to bring the leak rate down to 0.5 psi/hour or less, and so making sure that each section had less than 0.5 psi/hour was significant.

2.8.3 Methods of Leak Correction

To correct all of these leak problems, initially the group made sure to try and design the entire loop to be made up of stainless steel parts, fittings, and connections. From past experiments and experience in working with these connections, the project advisor and lab manager both suggested that stainless steel parts were the right course of action. Another way of correcting and minimizing leak was to check each bent tube to make sure the sleeves the aligned correctly and the compression fitting actually tightened into place, instead of at an angle. This was a big issue for the tubes going to the differential pressure transducers and at the corner curves on either side of the reservoir.

With most common correction techniques exhausted, the final step was to utilize Teflon tape. Each compression fitting was loosened from the loop and Teflon tape was added to secure the connection and minimize the leak further. By adding the tape and tightening to the maximum possible rotation, the leak rate of the entire setup was able to drastically improve from 5 psi/second, down to 0.3 psi/hour.

2.8.4 Charging the Reservoir

In order to being experimentation, step two of the experiment preparation involved charging the reservoir, meaning filling the reservoir with R-123. To fill the reservoir with the refrigerant, it was important to first remove it from the setup and figure out exactly how much fluid had to be in the reservoir. This was crucial because R-123 has a high expansion coefficient

when it comes in contact with vacuum, and when in two-phase experimentation, space would be required where the gas could expand.

First, a rough volume analysis of the loop was conducted using the simple formula of volume of a cylinder and using the different lengths of tubes at each of the sides. Even though other connections and a variety of sizes and shapes were involved, it was more important to get a rough estimate and multiply it by a large safety factor.

$$\text{Volume Analysis: } \left(\frac{d^2}{4}\pi\right)(\text{total length}) * \text{SafetyFactor} = \left(\frac{(0.18)^2}{4}\pi\right)(252) * 1.5$$

$$= 9.6189 \text{ in}^3 = 157.626 \text{ cm}^3(\text{cc})$$

Since it was known that the tank could hold a volume of around 900 cc and around twenty five percent of the tank had to remain empty to have enough room for expansion, the tank had to be filled with a maximum of around 600 cc. To fill the reservoir with refrigerant, the reservoir was initially weighed and the weighing scale was zeroed. Then vacuum was pulled using the Genco HYVAC 7, while having the virgin R-123 tank on an elevated surface as shown in the figure below. Finally, the valves were slowly opened and the weight being added was measured. Using a simple density relationship, it was calculated that the tank was filled up with 483.12 cubic centimeters of R-123, while the loop only required 157.63 cubic centimeters.

Figure 31: Elevated R-123 tank for filling the reservoir.

2.8.5 Pulling a Vacuum

Pulling a vacuum in the setup as well as reservoir was a significant step because it got rid of as much air as possible. Any air in the loop can cause bubbles and really affect the data negatively, causing problems with sensors and not allowing fluid to move through. Given the resources and machine in the lab, a simple vacuum was possible, and it was done using the Genco HYVAC 7 shown in the figure below. This machine was very sensitive and all changes had to be made at a very slow pace to make sure the oils didn't spill. In order to pull a vacuum, the machine had to be turned on and then the machine valve had to slowly be turned open until a change in noise occurred, and then there was a short period of waiting time until the noise disappeared and the valve continued to open. Similarly, the same was done for the reservoir valve, and the experimental loop. Once the valves were entirely open and being pulled into vacuum, the machine had to be left running for between thirty minutes to one hour.

Figure 32: Genco HYVAC 7 pulling a vacuum.

2.8.6 Filling the Experimental Loop

Once the reservoir and experimental loop were both in a vacuum, and the reservoir had been filled up, there was only one more step remaining which was to fill the loop the R-123 from the reservoir. In order to fill the loop, the valve from the reservoir to the loop was slowly opened and allowed to fill the corners of the setup for thirty minutes. After that, the mechanical pump was run for around thirty minutes with ice in the condenser to make sure that any R-123 which turned into vapor after getting in contact with vacuum, turned back to liquid phase after going through the loop several times. Once the experimental loop fill-up was completed, the setup was ready for running experiments.

Experimental Matrix

Below is a chart detailing all of the measurements taken during the flow distribution experiments conducted on the experimental setup. The scope of the project was limited to testing only for single phase conditions due to time constraints, so measurements such as heater voltage and power are not applicable for these experimental matrices, but may be in future applications.

Table 4: Experimental Variables.

Independent variables	Dependent variables
EHD Voltage	Total flow rate
Needle Valves (individual control of branch flow)	Temperature rise and drop of refrigerant
Mechanical pump flow rate	Quality of refrigerant
Heater Voltage	Pressure rise across pump
	Pressure drop across evaporator
	Heater Power

The main variables which could be directly controlled in the setup during experimentation were flow rate in each branch and the voltage delivered to the EHD pumps. Flow rate is established using the main external pump, but is also controlled by opening and closing the needle valves as well as the voltages applied to the EHD pumps. Pressure drop across each EHD pump is an important measurement for evaluating the performance of the EHD pumps, and is directly relate the voltage applied.

Variable Conditions and Ranges

Boundary conditions were set to determine the ranges of flow rate and EHD voltages to test through experimentation.

The flow rate in each branch was determined to be 1-15 mL/min. The flowmeters within each branch could only measure up to 50 mL/min, but consistent flows within branch was determined to be at a maximum of 20 mL/min. The individual EHD pumps could only generate a maximum flow rate of about 3 mL/min, so to be within safety, the range of flow rate in each branch was determined to be 1-15 mL/min.

The range of the voltages applied to EHD pumps was set to 0-1500V. From previous experiments, the maximum voltage applied was 1500V, as fluid breakdown and sparks in pumps was found in higher voltages.

Basic Experimental Procedure

Voltage Stepping

In each experiment with the EHD pumps activated, data was collected in increments of 100V. Starting from 0V, the applied voltage was increased in steps of 100 V until reaching a maximum of 1500V, at which point it was then decreased back down to 0V, similarly in increments of 100V. At each voltage step, the team had the opportunity to check if it was safe to proceed by observing any sounds that would indicate sparks.

Data Recorded

In these single phase experiments, data was collected from voltage applied in each EHD pump, current applied in each EHD pump, flow rate in each branch, absolute pressure at the merging of the branches, and pressure rise across the EHD pumps. Additional data collected

from the setup, but was not essential to understanding the single phase data, was temperature at inlets and outlets of the EHD pumps, temperature at each inlet and outlet of the micro channels, temperature at the reservoir and condenser, and pressure drop across the channels.

Experiment I: Static Condition

Pump performances were evaluated in static condition, with both valves closed and the mechanical pump off. Pumps were activated one at a time, increasing and then decreasing by 100V on a range of 0-1500V. This experiment provided pressure generation data for each of the EHD conduction pumps.

Table 5: Pump Performance Experimental Matrix.

Overall Flow Rate [mL/min]	Valve 1	Valve 2	EHD Pump 1	EHD Pump 2
N/A	Closed	Closed	Activated	Off
N/A	Closed	Closed	Off	Activated

Experiment II: Pump Performance

Individual EHD pump performances were determined by opening and activating only one of the branches. One branch would be closed by the needle valve, leaving the other branch open. This open branch was then activated, increasing and then decreasing by 100V. This experiment was essential to determining the pump performance and can be carried forward in next experiments.

Table 6: Pump Performance Experimental Matrix.

Overall Flow Rate [mL/min]	Valve 1	Valve 2	EHD Pump 1	EHD Pump 2
1.0	Open	Closed	Activated	Off
2.0	Closed	Open	Off	Activated

Experiment II: Equal Distribution to Maldistribution

This experiment tested individual pump's ability to create differences in the flow rate within each branch. Both valves in each branch were opened, but only one EHD pump will be activated at a time.

The external pump would first establish a desired total flow rate within the loop and the needle valves were adjusted to create equal flow rates within each branch. Once equal flow distribution was found, one of the EHD pumps was activated and carefully gone through the voltage stepping. The objective was to observe the changes in flow distribution in each of the branches and the actual differences in flow rates between the branches. Multiple iterations of the experiment were gone through, with each trial starting at a different initial total flow rate.

Table 7: Equal to Maldistribution Experimental Matrix.

Overall Flow Rate [mL/min]	Branch 1 Flow Rate [mL/min]	Branch 2 Flow Rate [mL/min]	Valve 1	Valve 2	EHD Pump 1	EHD Pump 2
10	5	5	Open	Open	Activated	Off
10	5	5	Open	Open	Off	Activated
15	7.5	7.5	Open	Open	Activated	Off
15	7.5	7.5	Open	Open	Off	Activated
20	10	10	Open	Open	Activated	Off
20	10	10	Open	Open	Off	Activated

Experiment III: Maldistribution to Equal Distribution

This experiment tested the pumps' ability to return the flow back to equal distribution between each of the two branches after forcing maldistribution in the two branches.

The external pump would first establish a total flow rate within the loop, but the valve would be adjusted to see a 1mL/min difference in each of the branches. After the distribution of flow rates was settled, one of the EHD pumps would be activated and go through the voltage stepping. This experiment would be repeated for the next pump as well. Likewise for experiment II, this experiment would be repeated for different total flow rates established from the external pump.

Table 8: Mal to Equal Distribution Experimental Matrix.

Overall Flow Rate [mL/min]	Branch 1 Flow Rate [mL/min]	Branch 2 Flow Rate [mL/min]	Valve 1	Valve 2	EHD Pump 1	EHD Pump 2
10	5.5	4.5	Open	Open	Activated	Off
10	5.5	4.5	Open	Open	Off	Activated
15	8	7	Open	Open	Activated	Off
15	8	7	Open	Open	Off	Activated
20	10.5	9.5	Open	Open	Activated	Off
20	10.5	9.5	Open	Open	Off	Activated

Chapter 3: Results and Discussion

3.1 Experiment I: Static Conditions

The first experiment conducted to understand the EHD pump's performance was activating the pumps with the branches completely closed to observe pressure generation in the absence of flow. Both branches were completely closed with the needle valves and activated only the EHD pump in branch 2. Data collection started once the flow in both branches was observed to negligible.

Three trials of this experiment was run, two where the voltage stepping was from 0-1500 V and one with the voltage dropping from 1500 V to 0 V. The obtained measurements was EHD voltage and the resulting pressure generation from the activated EHD pump.

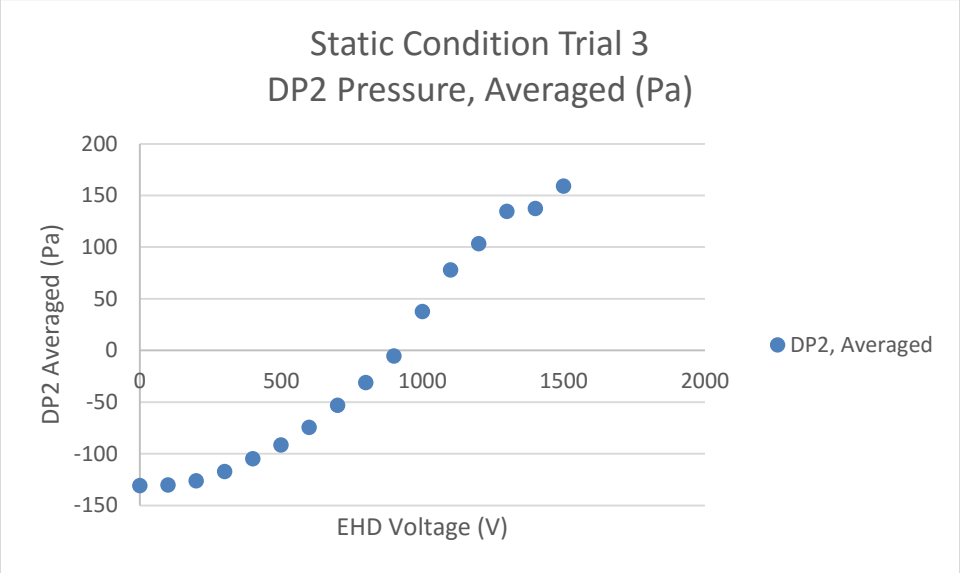

Figure 33: Static Condition: EHD Voltage vs. Differential Pressure across Branch 2, Trial 3

This data matched the theoretical pump performance curves we anticipated, with a polynomial curve fit of the pressure generation as a direct product of applied voltage. The observed pressure generation across the entire range was 280 Pascals, which is similar to the results of the previous year's experiment, confirming that the EHD pump is still as active.

3.2 Experiment II: Dynamic Pump Performance Test

Once again these tests were only performed on the only operating EHD pump in the loop. The corresponding branch (branch 2) was opened completely while branch 1 was left closed. Only two trials of this experiment was conducted, once with voltage stepping up from 0 V to 1500 V and the second stepping down from 1500 V to 0 V. The collected data analyzed was the EHD voltage across the pressure generation of the activated pump, and the EHD voltage vs. the change in flow rate.

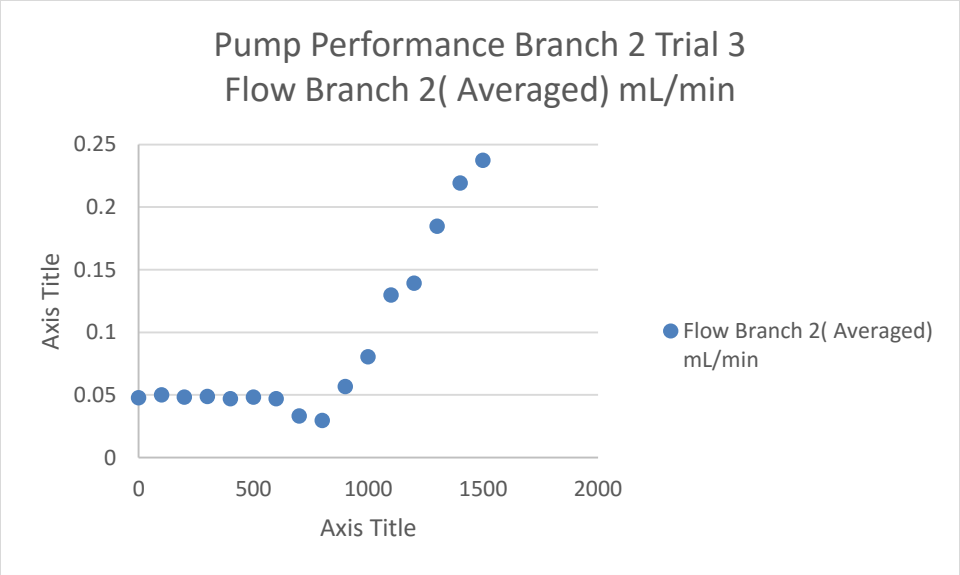

Figure 34: Pump Performance Curve: EHD Voltage vs. Pump Performance (mL/min) in Branch 2, Trial 3

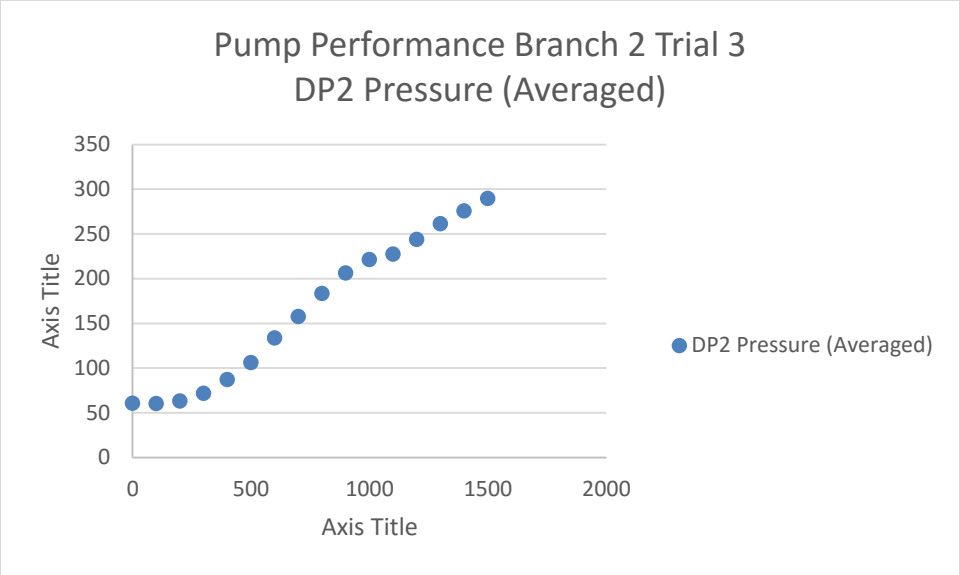

Figure 35: Pump Performance Curve, EHD Voltage vs. Differential Pressure in Branch 2, Trial 3

The graphs above indicate there is a positive direct relation of voltage applied to both flow rate and pressure generation across the EHD pump. The performance curve of the pressure generation is similar to the above static condition results, with a total pressure generation of 230 Pascal, even matching the S-shaped fitted curve. The minimal pressure and flow rate rise might be influenced by the channels being micro scaled but extended over a long length, and why so much voltage was required to rise the flow rate at all. This results did conclusively confirmed the EHD conduction phenomena that the Coulomb's force could sufficiently create pressure generation.

3.3 Experiment III: Equal Flow to Maldistribution

While only one EHD pump was available for experimentation, it was still possible to operate one pump across two open branches. This was the first experiment that the mechanical pump was required, so flow can be initialized in the entire branch for flow to be observed to change. The needle valves were coordinated to set the flow to allow for approximately 0.9

mL/min in each branch. The data collected from this experiment was the flow rates in both branches and the differential pressures across each pump vs. the EHD voltages. Due to time constraints, only one trial was conducted (voltage stepping from 0V to 1500V).

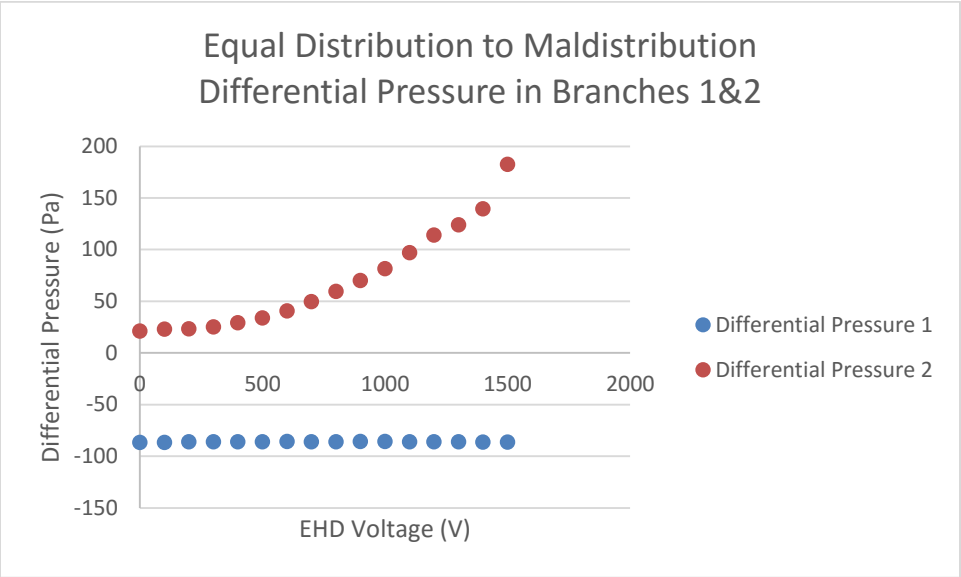

Figure 36: Flow Distribution, Equal to Maldistribution: EHD Voltage vs. Differential Pressures in Branch 1&2

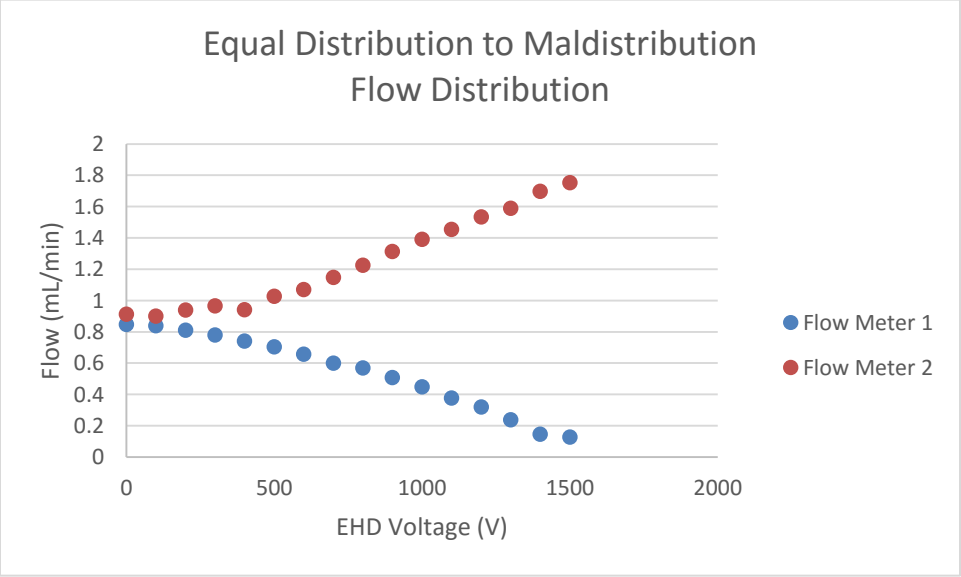

Figure 37: Flow Distribution: Equal to Maldistribution, EHD Voltage vs. Flow Rate (mL/min) in Branches 1 & 2

The pressure generation curves are misleading as they were not zeroed to the same value, but the essential observation from these curves is that even though flow was altered in both branches, only the activated branch saw any pressure rise. The flow in both branches saw nearly identical (quadratic) curves of change flow just in opposite directions, showing that the EHD pump could effectively draw out fluid from one parallel branch to another for increased demand. This is promising for the application of EHD pumping for flow distribution.

3.4 Experiment IV: Maldistribution to Equal Distribution

This experiment was fundamentally similar to the one above, except we intentionally create a difference of flow in the branches of 1 mL/min by using the needle valves to distribute the flow. For this experiment, because only the EHD pump in branch 2 was operational, the flow was favored toward branch 1. The theory was that by increasing the voltage in branch 1 the flows would eventually converge. The observed measurements were also flow rate between each branches and the pressure generation across each of the EHD pumps (activated or not) as the EHD voltage was varied. The results initially were promising, but proved to be inconclusive as the flow distribution converged until 500 V, where higher voltages progressively caused the flow distribution to worsen. This data was possibly skewed from blockage somewhere within the second branch that counteracted the increased pressure generation of the EHD pump.

3.5 Potential Causes of Error

The period of experimentation for this project was given a compressed timeline because of constant technical problems during assembly and leak testing of the loop. The experiments conducted were done in only one branch because the performance of one of the EHD pumps was malfunctioning due to either lack of connectivity of electrodes or unforeseen electrical

connection issues. If given a longer timeframe, this group would've tried to disassemble the loop to investigate and correct for the error in the malfunctioning EHD pumps.

Results may have also been affected by excess air or debris in the loop. It was consistently difficult to completely draw a vacuum from the loop, and based on our absolute pressure and temperature measurements, it was possible that compressed air was trapped in the loop. Additionally, even though the tank of R123 drawn from to charge the reservoir was labeled virgin, it was still necessary to filter the refrigerant. Undesirable particles could've permeated into the loop and created blockage to prevent smooth flow.

The pressure transducers used in the loop have been in reuse for many years, and the wear could have presented errors in our differential pressure measurements. This is a possible explanation for errors encountered with pressure measurements when the EHD pumps exceeded outputting 1200 V.

Conclusion

The intent of this Major Qualifying Project was to investigate the application of EHD conduction pumping for the purposes of controlling flow distribution in micro-scale parallel channels. Although the planned goal of the MQP was also to research in junction with heat transfer applications for two phase flow, this was not achieved due to time constraints. Instead, the group was able to design and assemble a setup capable of running both single and two phase experiments. The results from the experiments show that micro-scale EHD conduction pumping can generate sufficient pressure level to distribute flow in parallel micro-channel applications. Additionally the project succeeded in gathering performance data on previously used EHD pumps, which despite being in continuous use for many years, still proved to perform sufficiently after simple maintenance checks, cleaning, and confirmation of electrode connections. Finally the project established a foundation for further research by means of the constructed experimental setup which will be able to collect two phase data on the effects of phase change on the pumping performance and the capacity of EHD conduction to provide efficient heat transfer in parallel micro-channel applications.

References

[1] J. Seyed-Yagoobi, 2005, “Electrohydrodynamic pumping of dielectric liquids”, Journal of Electrostatics, vol. 63, pp. 861-869.

[2] M. R. Pearson, J. Seyed-Yagoobi, 2009, “Advances in Electrohydrodynamic Conduction Pumping”, IEEE Transactions on Dielectrics and Electrical Insulation, vol. 16, pp. 424-434.

[3] Y. Feng, J. Seyed-Yagoobi, 2004, “Control of Liquid Flow Distribution Utilizing EHD Conduction Pumping Mechanism”, Conference Record of the 39th IEEE IAS Annual Meeting, vol. 4, pp. 2345-2352.

[4] P. Atten, J. Seyed-Yagoobi, 2003, “Electrohydrodynamically Induced Dielectric Liquid Flow Through Pure Conduction in Point/Plane Geometry”, IEEE Transactions on Dielectrics and Electrical Insulation, vol. 10, no. 1, pp. 27-36.

[5] V. K. Patel, F. Robinson, J. Seyed-Yagoobi, 2013, “Terrestrial and Microgravity Experimental Study of Microscale Heat-Transport Device Driven by Electrohydrodynamic Conduction Pumping”, IEEE Transactions on Industry Applications, vol. 49, pp. 2397-2401.

[6] V. K. Patel, J. Seyed-Yagoobi, 2011, “Dielectric fluid flow generation in meso-tubes with micro-scale electrohydrodynamic conduction pumping”, Proceedings of the IEEE International Conference on Dielectric Liquids, pp. 1–4.

[7] M. R. Pearson and J. Seyed-Yagoobi, “Experimental study of EHD conduction pumping at the meso- and micro-scale”, Journal of Electrostatics, vol. 69, pp. 479-485.

[8] C. Jiang, K. Minchev, B. Shaw, 2015, “Flow Generation and Distribution Control in Meso Scale via Electrohydrodynamic Conduction Pumping”, Worcester Polytechnic Institute Major Qualifying Project Database.

[9] Glenn Brown, 2000, “Henry Darcy and His Law, The Darcy-Weisbach Equation”, Oklahoma State University, https://bae.okstate.edu/faculty-sites/Darcy/DarcyWeisbach/Darcy-WeisbachEq.htm

[10] Precision Coating, 2015, “Benefits of Teflon (PTFE) Coatings”, Grant Marketing, http://precisioncoating.com/fluoropolymer-coatings/benefits-of-teflon-ptfe-coatings/

[11] Sensirion, 2016, “SLI-Flow Meters for Life Science and Automation”, https://www.sensirion.com/products/precise-liquid-flow-sensors-for-low-flow-rates/slx-series/universal-liquid-flow-sensor-for-life-science-and-automation/

[12] Validyne Engineering, 2016, “DP15 Variable Reluctance Pressure Sensor Capable of Range Changes”, DreamSoft IT Solution, http://validyne.com/product/DP15_Variable_Reluctance_Pressure_Sensor_Capable_of_Range_Changes#sthash.KYWRcuT9.dpbs

[13] First Sensor AG, 2016, “Understanding the difference between absolute, gage, and differential pressure”, http://www.first-sensor.com/en/products/pressure-sensors/pressure-sensors-and-transmitters/pressure-types.html

[14] V. K. Patel, F. Robinson, J. Seyed-Yagoobi, 2013, “Terrestrial and Microgravity Experimental Study of Microscale Heat-Transport Device Driven by Electrohydrodynamic Conduction Pumping”, IEEE Transactions on Industry Applications, vol. 49, pp. 2397-2401.

Appendices

Appendix A: Assembly Loop Solid Models

Full Loop Assembly

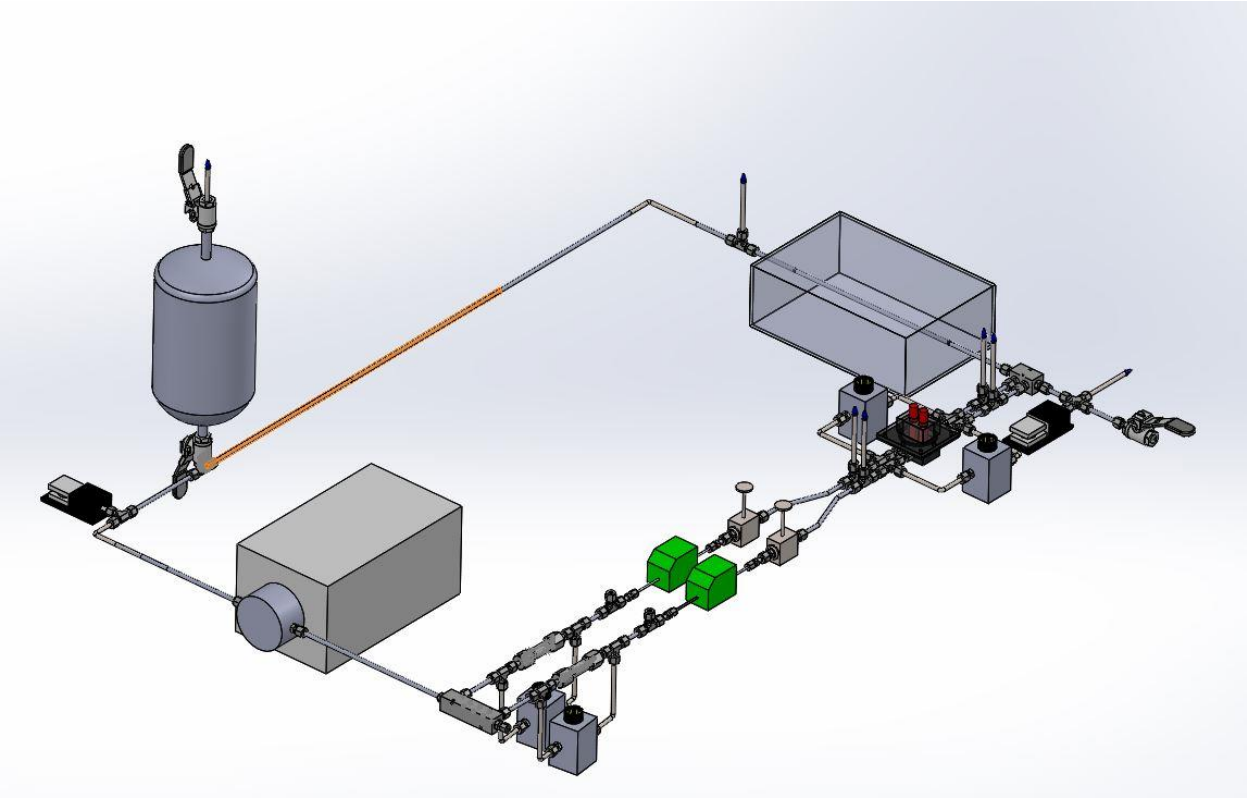

Section 1: Evaporator Side

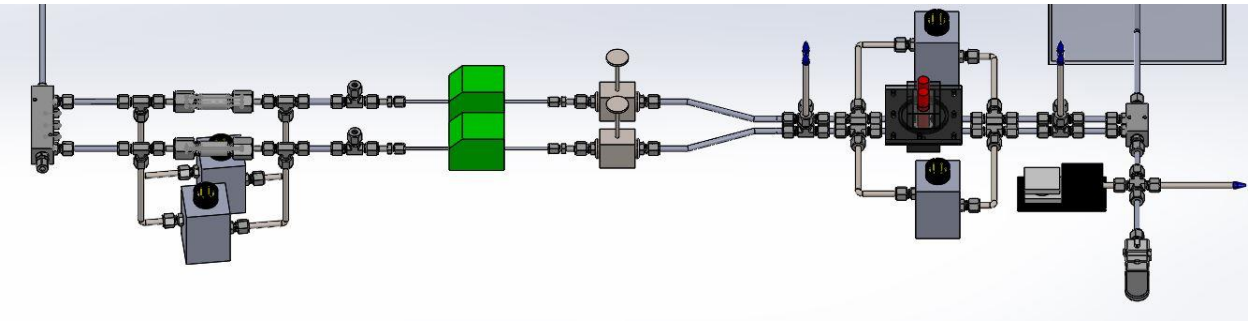

Section 1: Evaporator Side – EHD Pumps

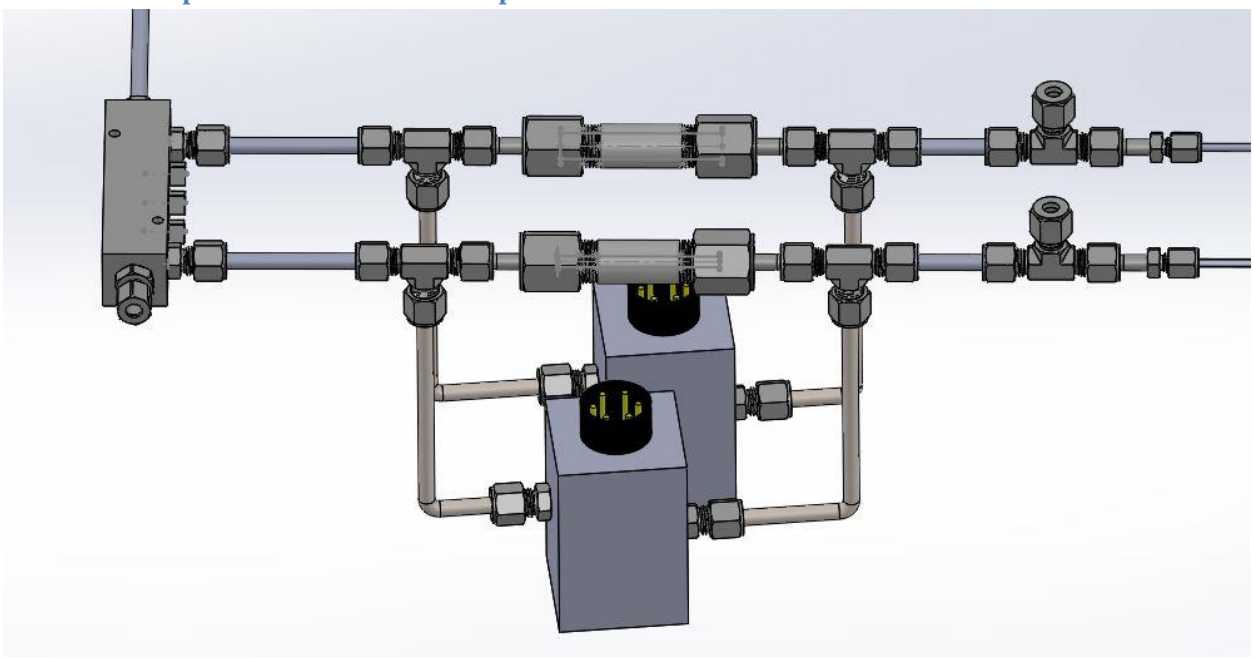

Section 1: Evaporator Side – Flowmeters

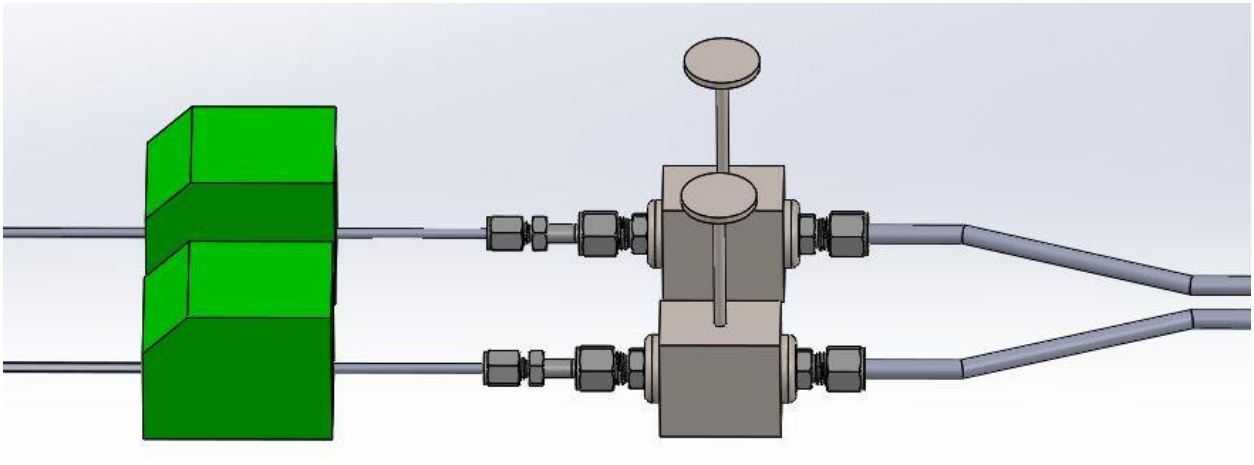

Section 1: Evaporator Side – Evaporator

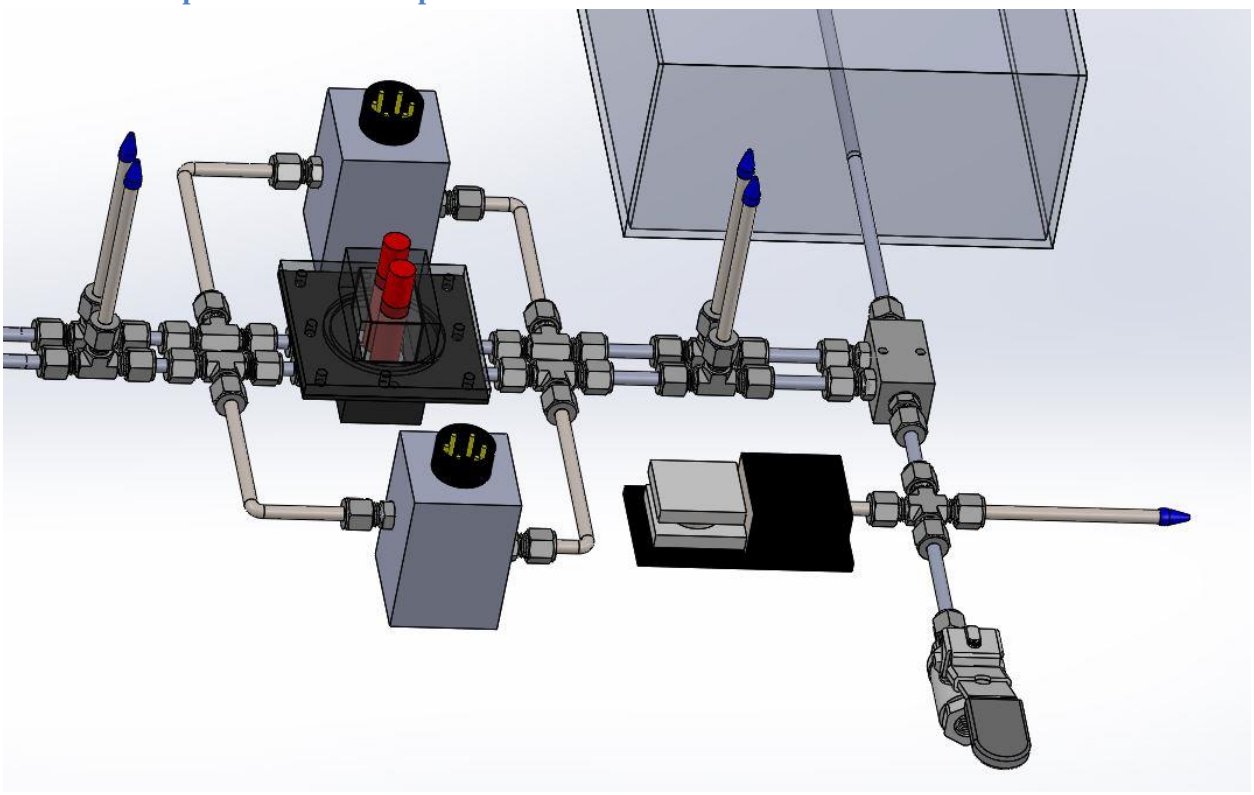

Appendix B.1: Differential Pressure Transducers Calibration Curves

Differential Pressure Transducer 1

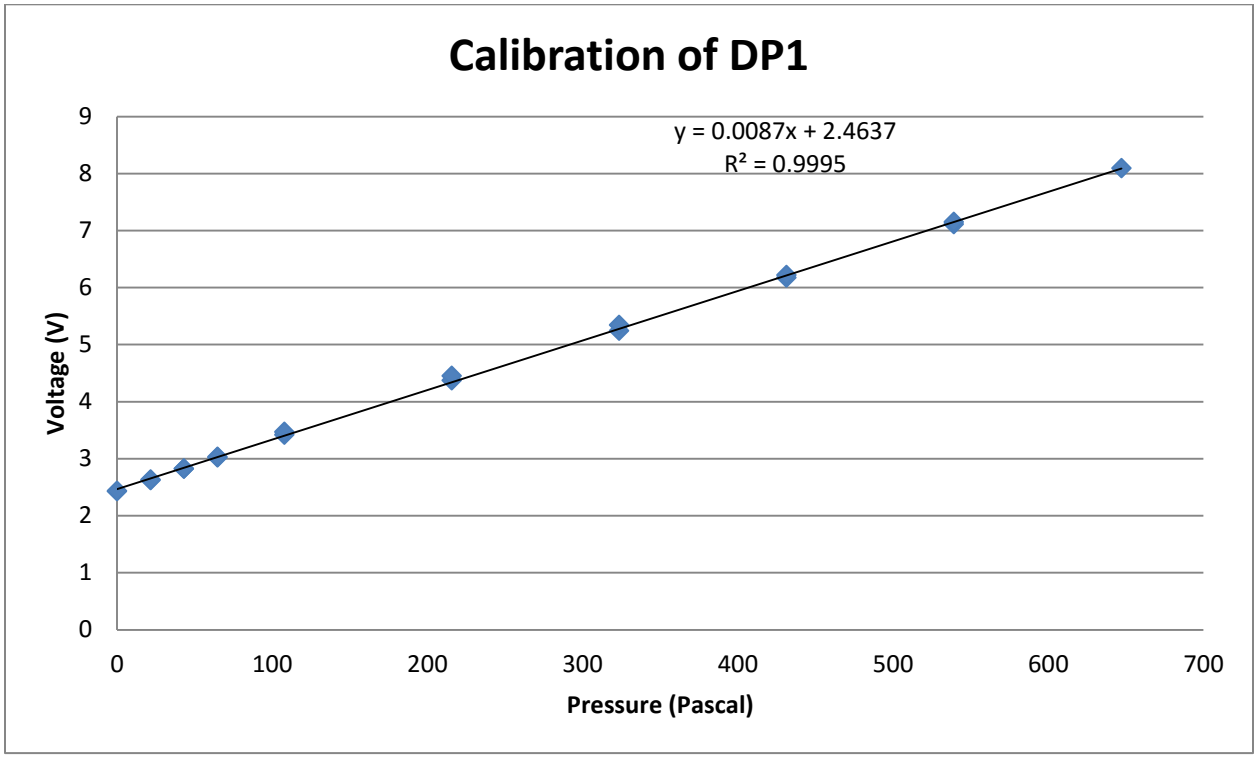

Differential Pressure Transducer 2

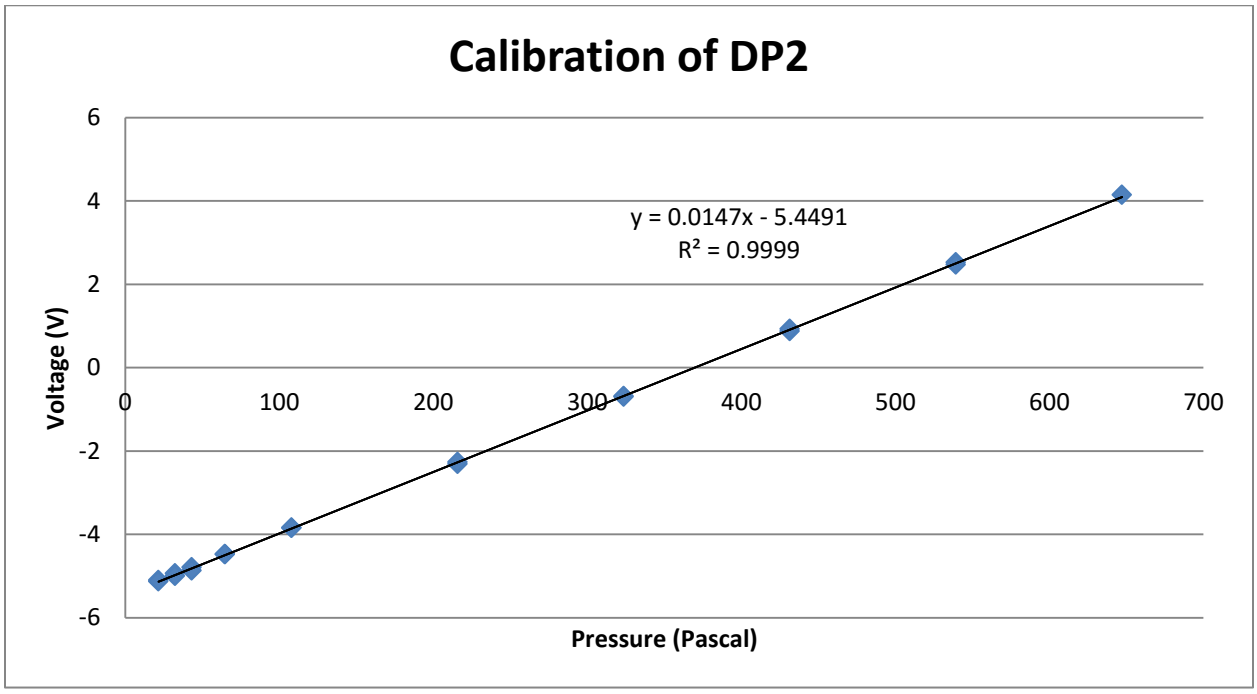

Differential Pressure Transducer 3

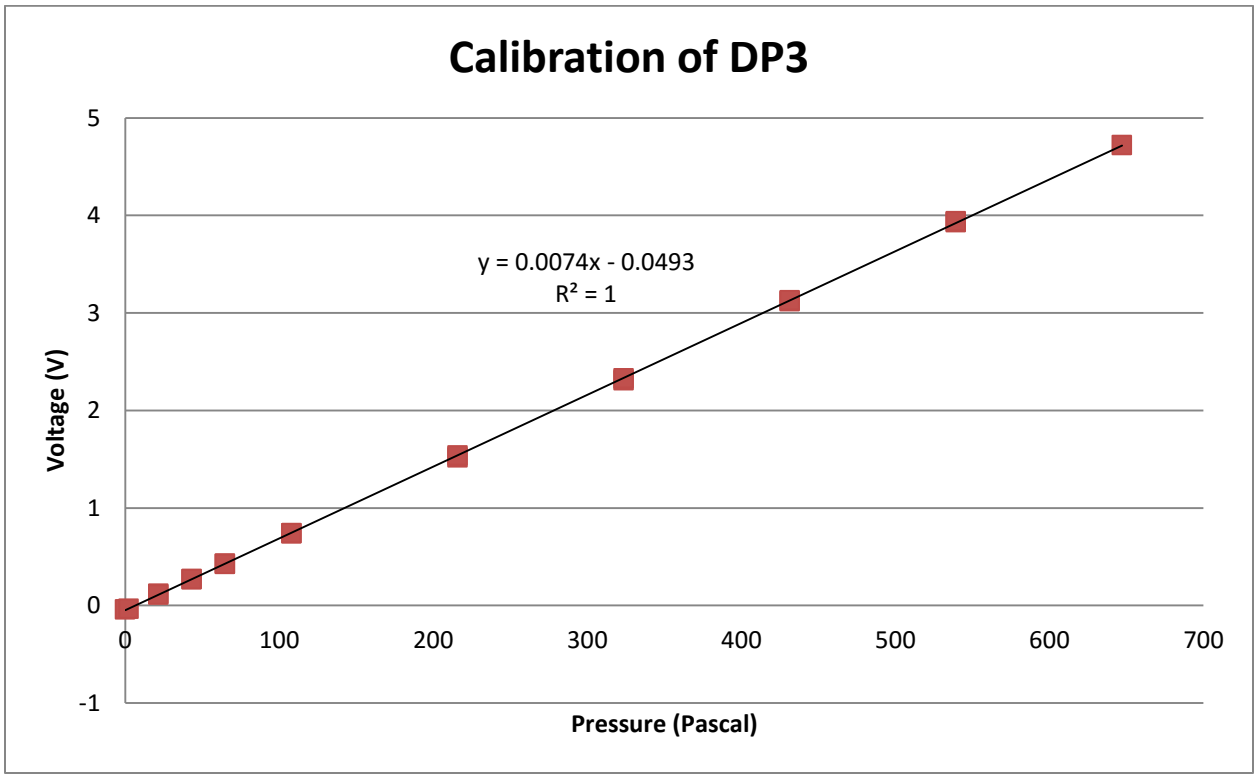

Differential Pressure Transducer 4

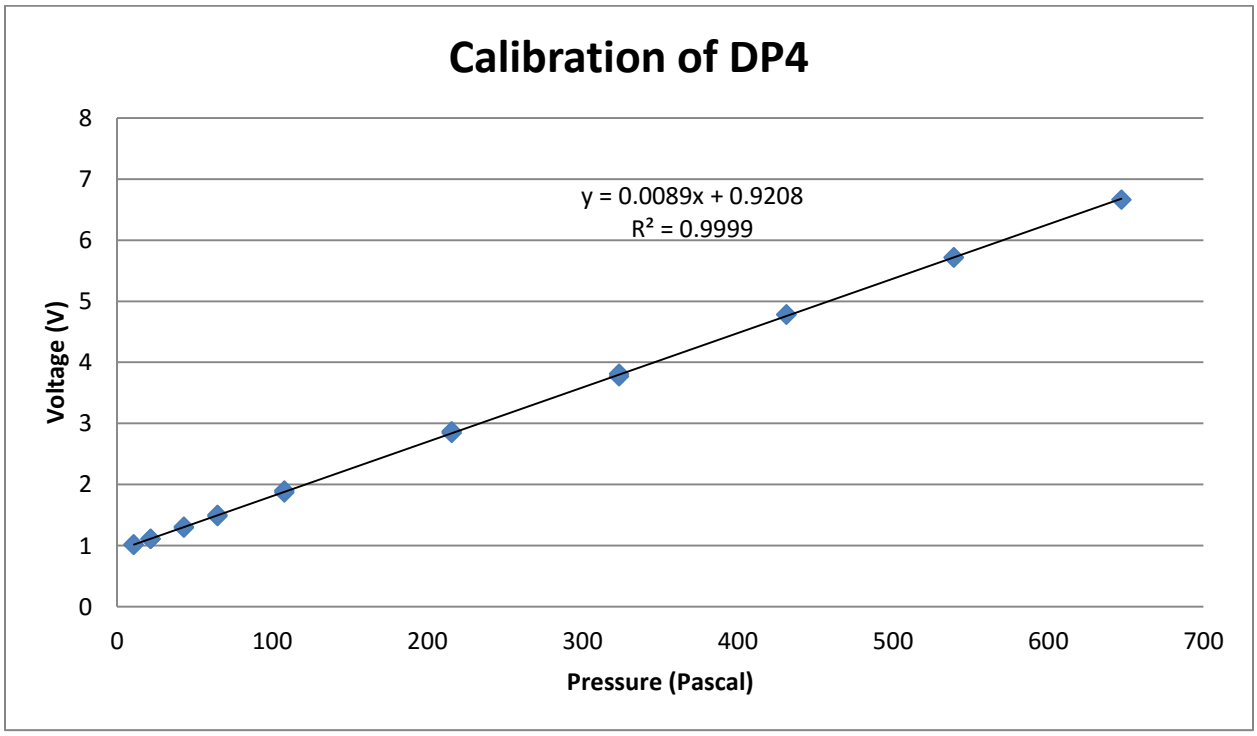

Appendix B.2: Flowmeters Calibration Curves

Flowmeter 1

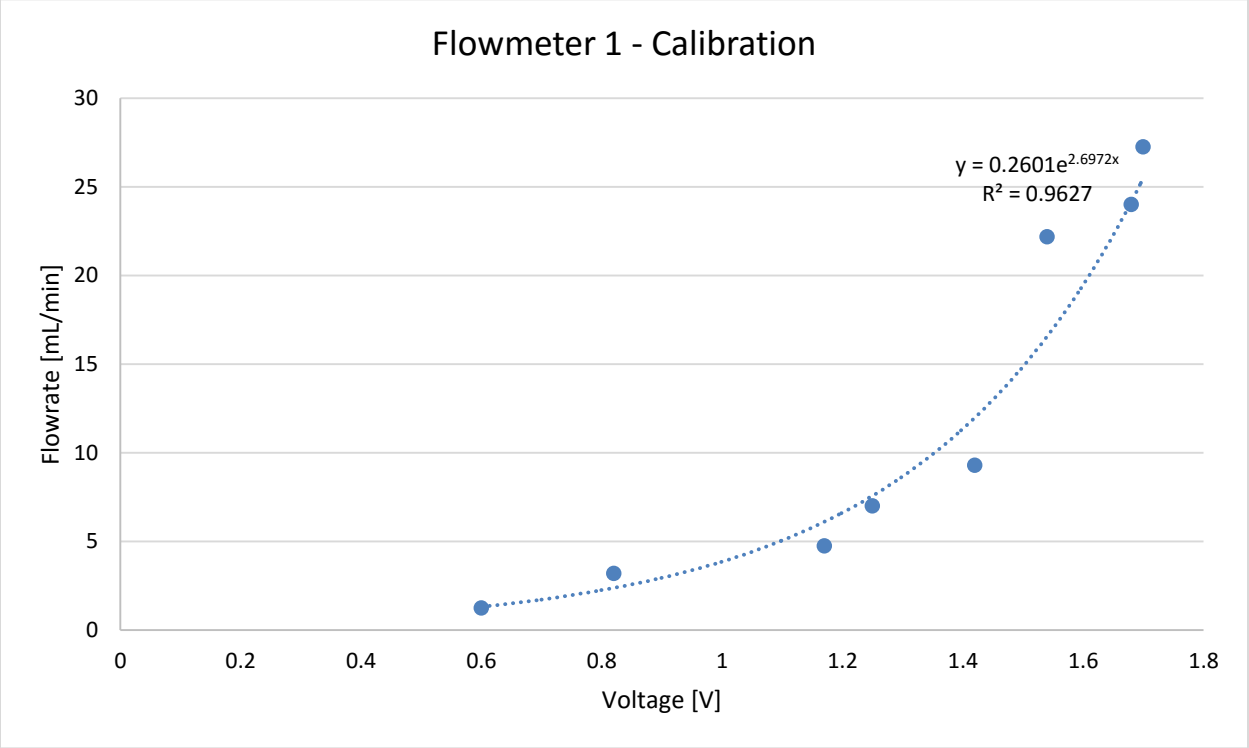

Flowmeter 2

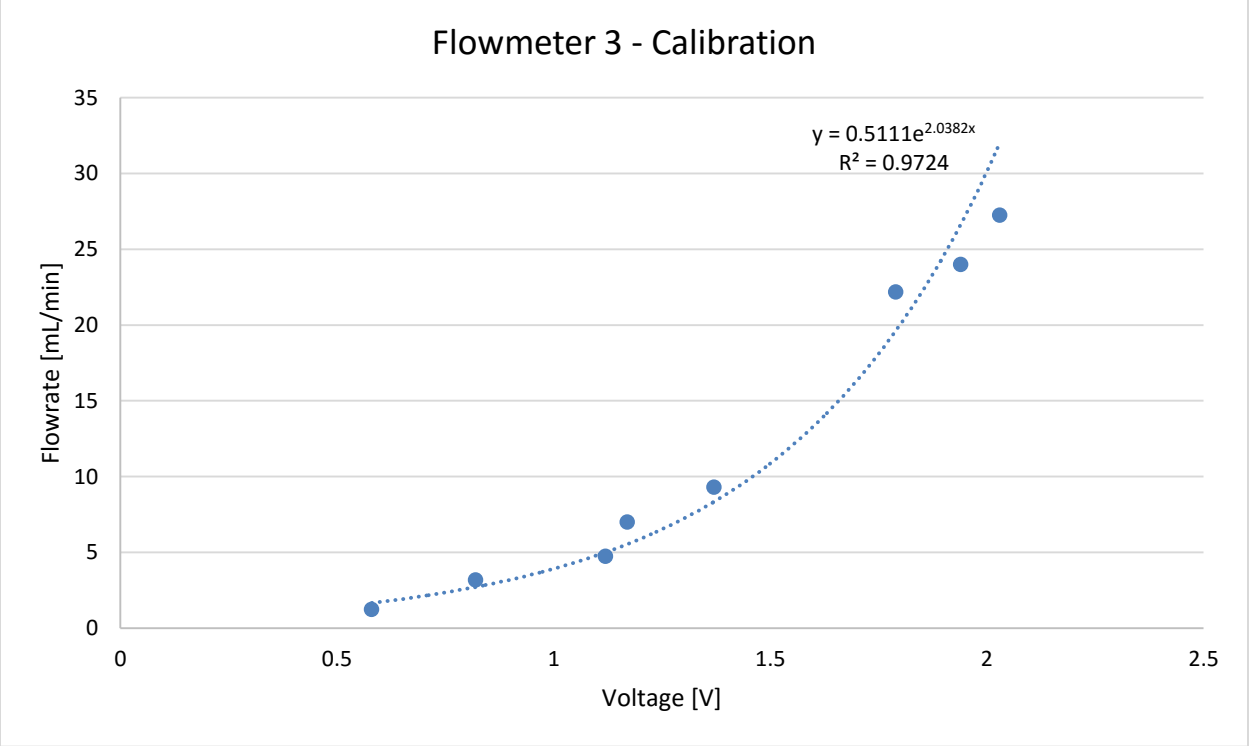

Appendix C.1: LabVIEW Block Diagram

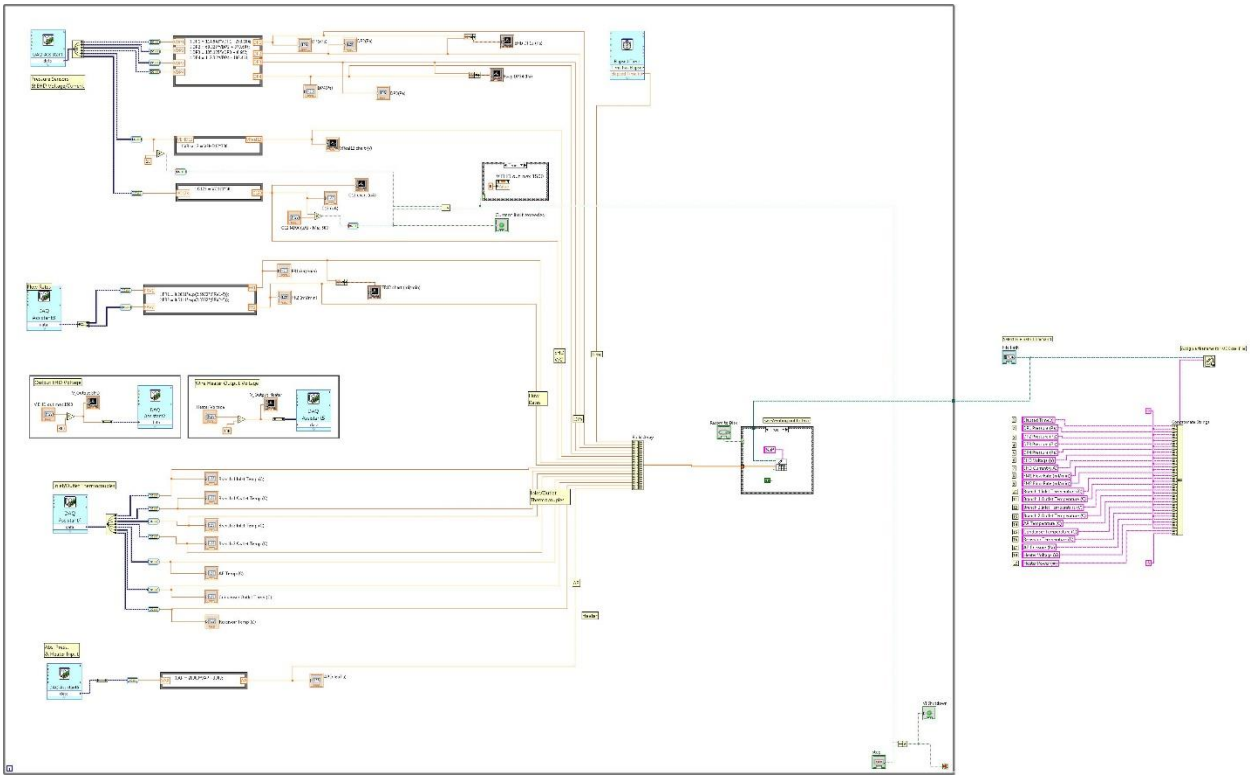

Appendix C.2: LabVIEW User Interface

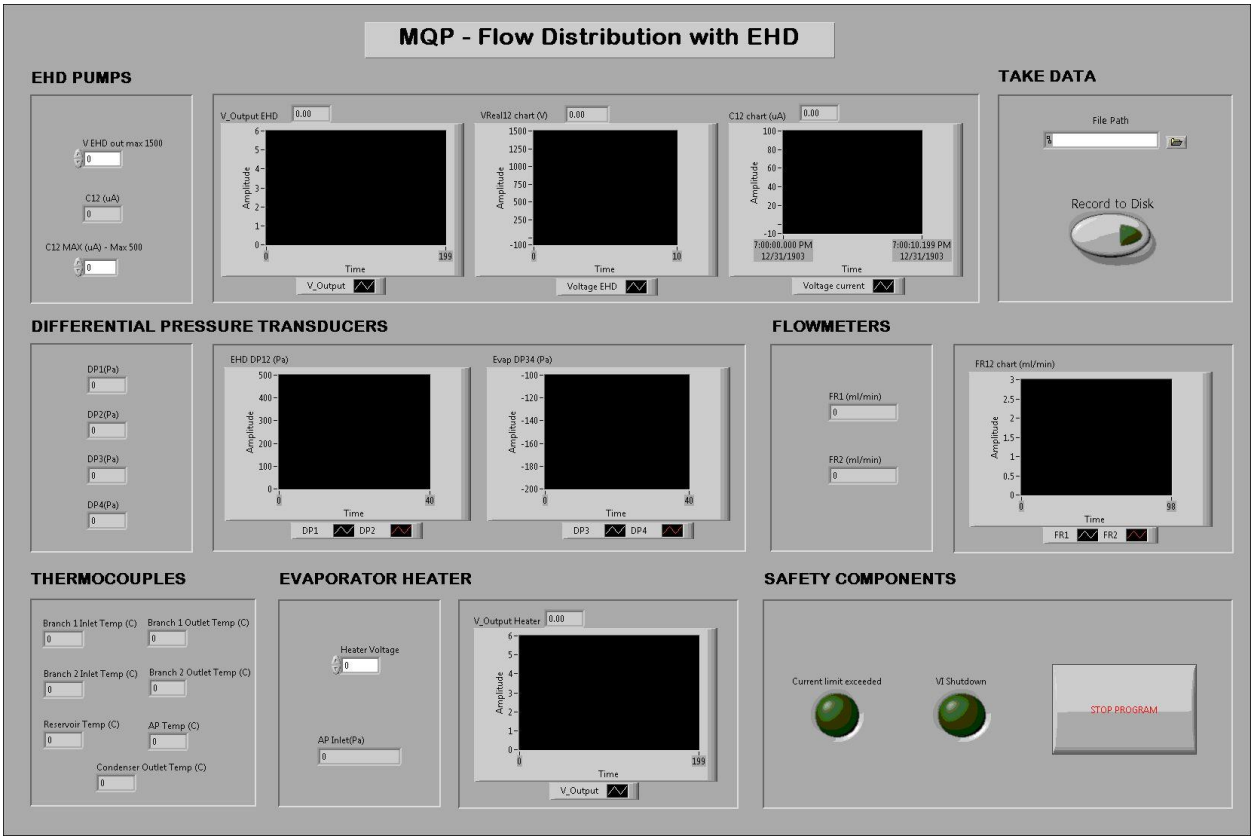

Appendix D.1: Thermocouple Probe Configuration

Thermocouple Probes	Location	DAQ Box	Channel
TP 1	Branch 1 Inlet	NI – USB – 9213	ai8
TP 2	Branch 1 Outlet	NI – USB – 9213	ai10
TP 3	Branch 2 Inlet	NI – USB – 9213	ai9
TP 4	Branch 2 Outlet	NI – USB – 9213	ai11
TP 5	AP	NI – USB – 9213	ai13
TP 6	Condenser Outlet	NI – USB – 9213	ai12
TP 7	Reservoir	NI – USB – 9213	ai7

Appendix D.2: Flowmeters Configuration

Flowmeters	Location	DAQ Box	Channel
FM 1	Branch 1	NI – USB – 6009	ai4
FM 2	Branch 2	NI – USB – 6009	ai5

Appendix D.3: Differential Pressure Transducers Configuration

Differential Pressure Transducer	Location	DAQ Box	Channel
DPT 1	Branch 1 EHD	NI – PCS	ai5
DPT 2	Branch 2 EHD	NI – PCS	ai2
DPT 3	Branch 1 Evap	NI – PCS	ai3
DPT 4	Branch 2 Evap	NI – PCS	ai4

Appendix D.4: EHD Pump Voltage/Current Supply Configuration

EHD Voltage Source	DAQ Box	Channel
Voltage	NI – PCS	ai7
Current	NI – PCS	ai6

Appendix E.1: Experimental Test Curves

Static Condition – Trial 1

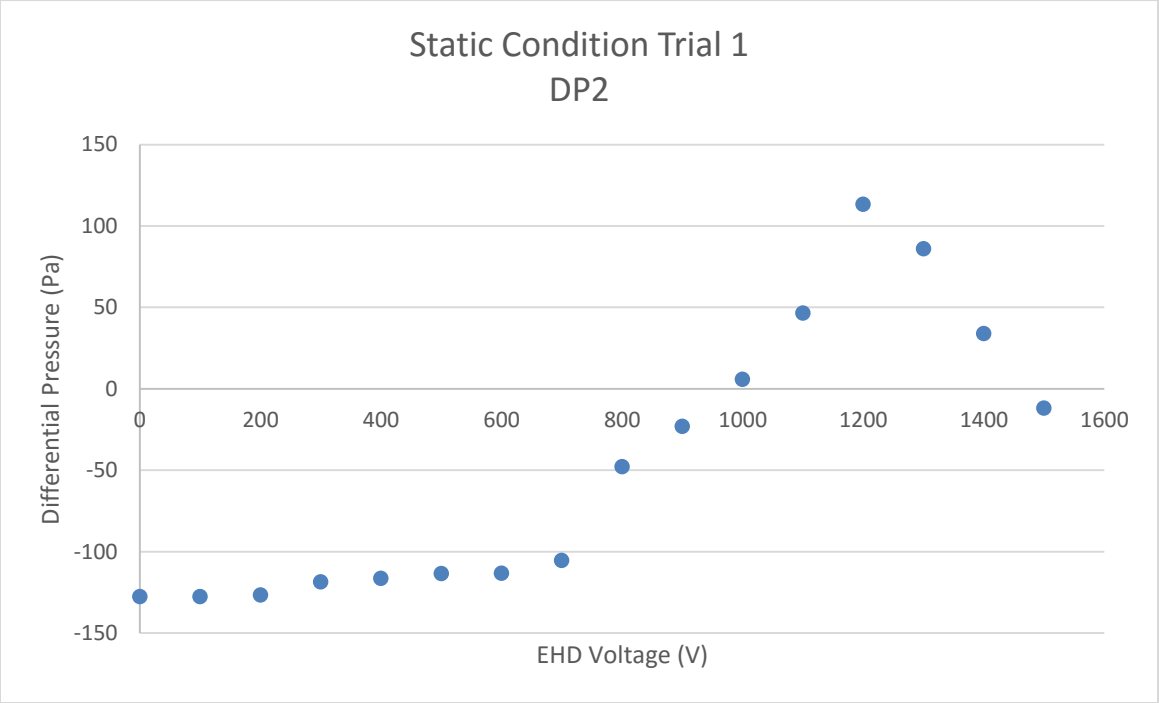

Static Condition – Trial 2

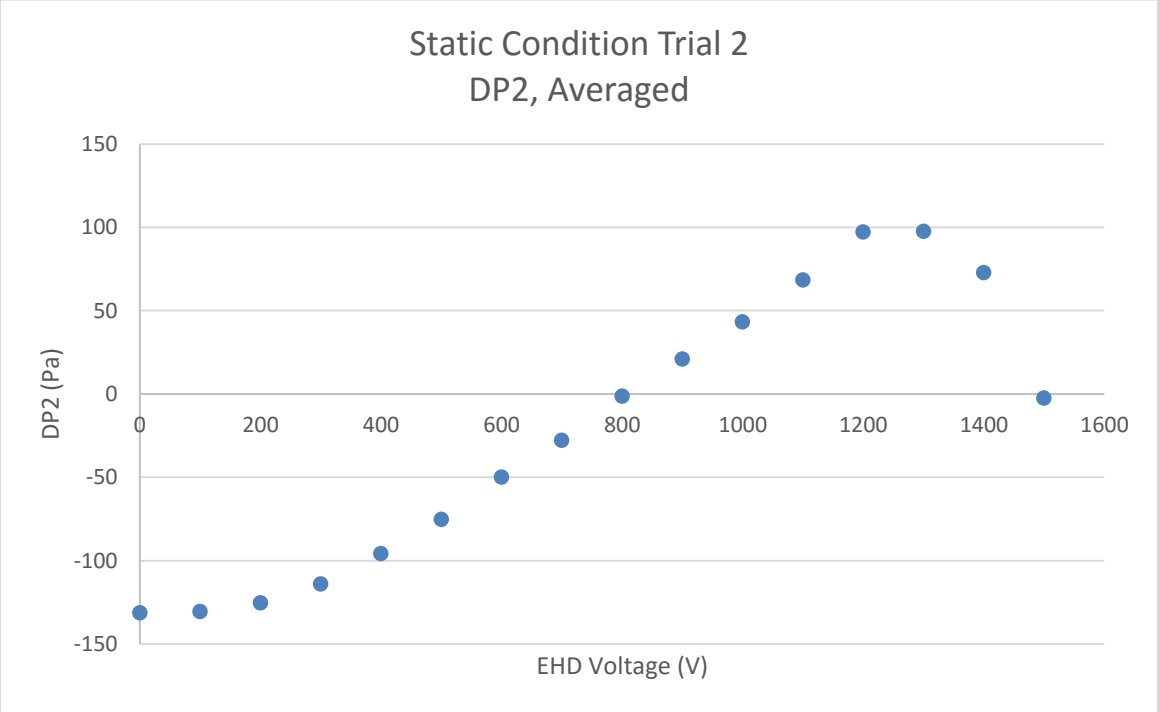

Static Condition – Trial 3

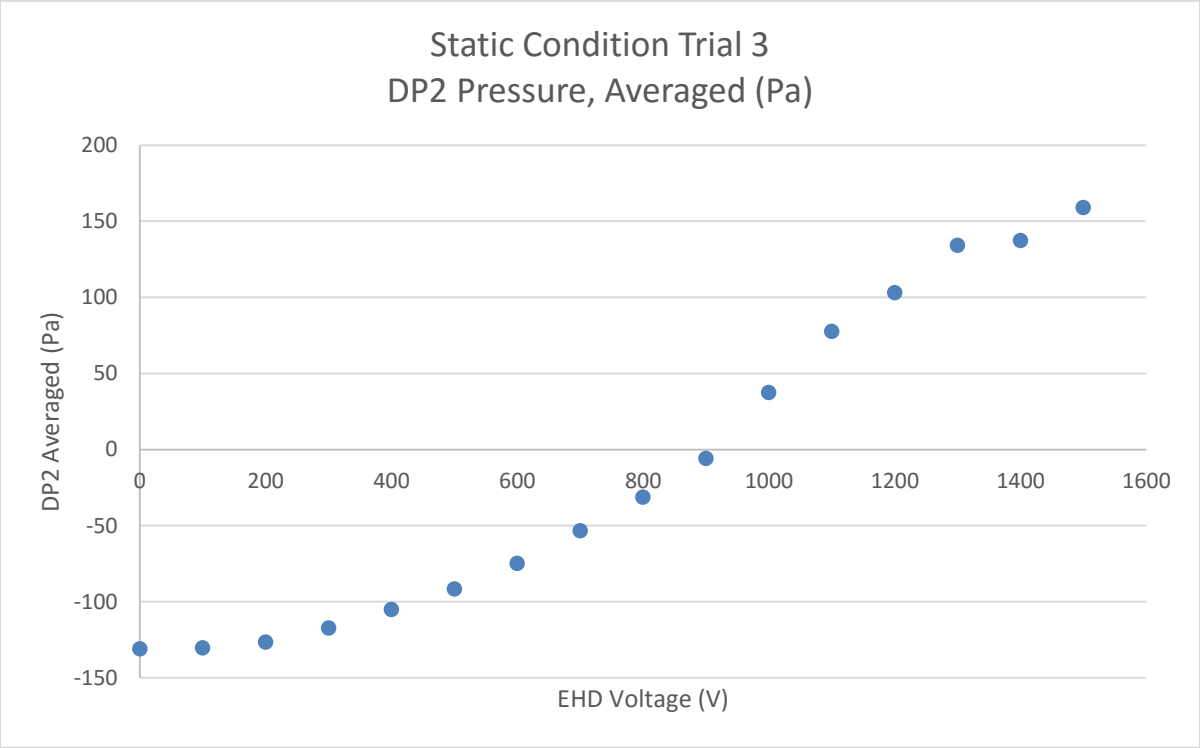

Pump Performance – Trial 2

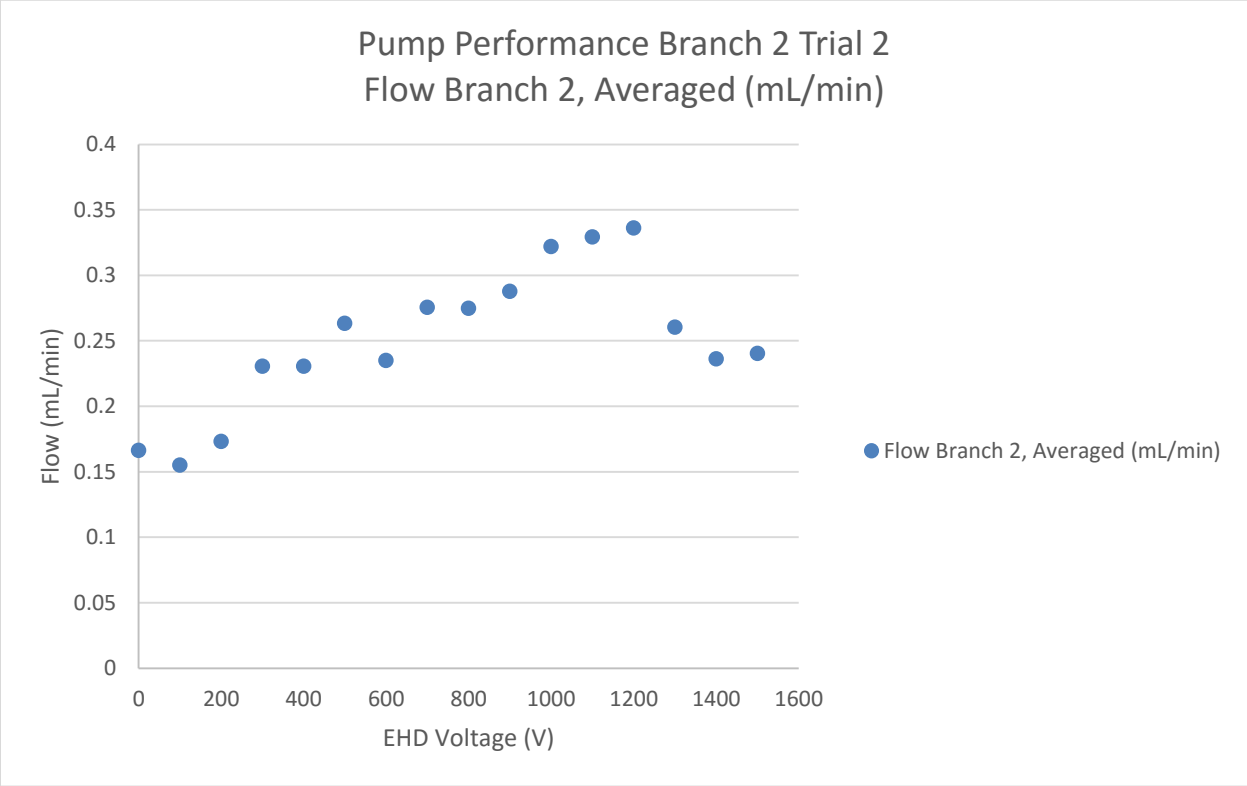

Static Condition – Trial 3

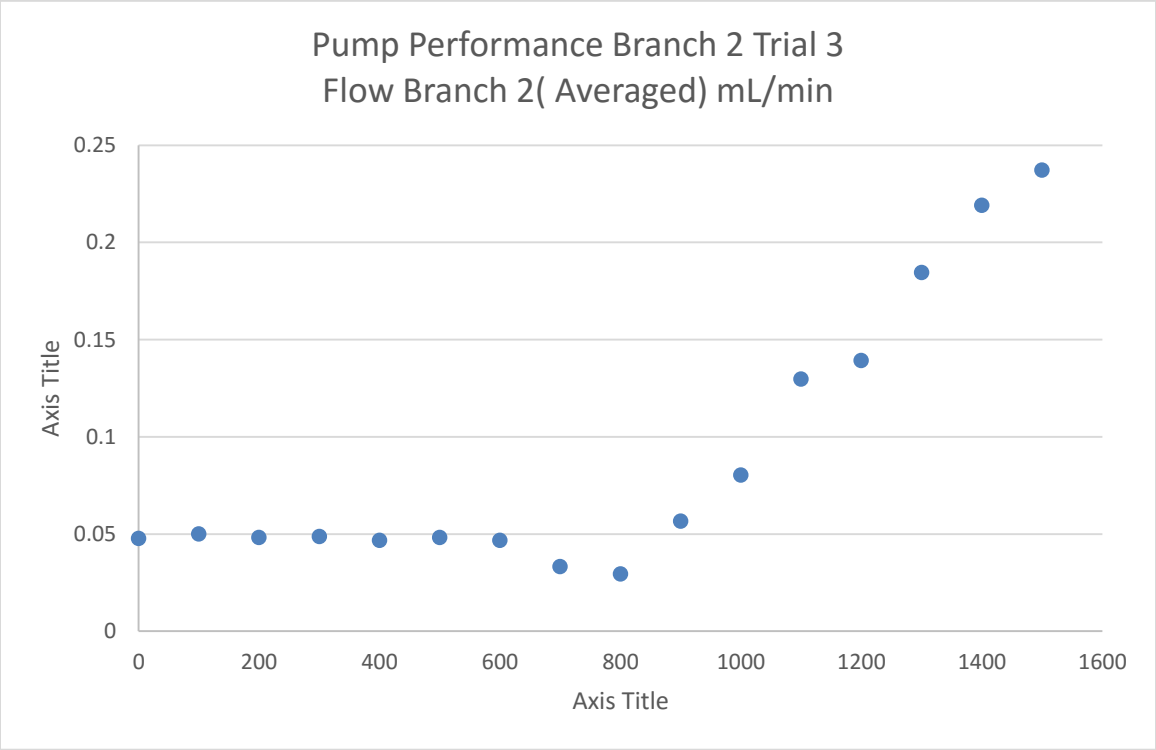

Equal Distribution to Maldistribution

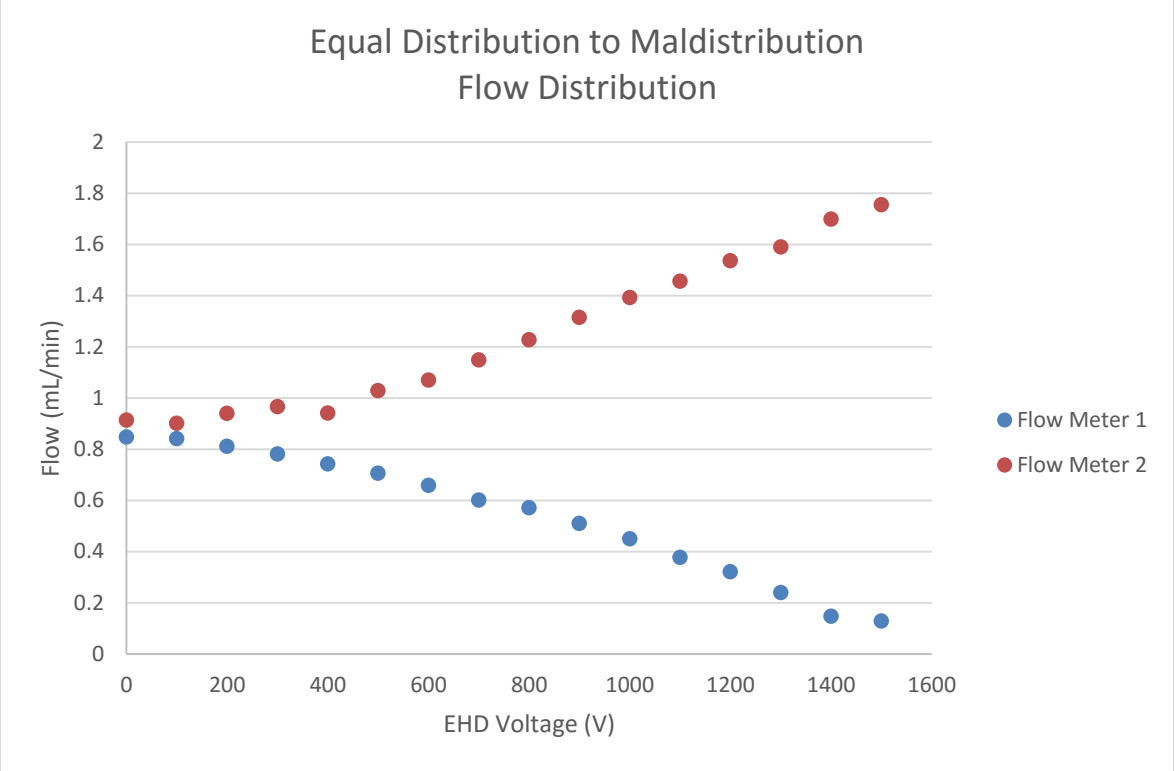

Appendix F: Physical Properties of R-123

Physical Properties

Chemical Formula	$CHCl_2CF_3$	
Molecular Weight	152.93	
Boiling Point at One Atmosphere	82.0°F	(27.85°C)
Critical Temperature	362.63°F 822.30°R	(183.68°C) (456.83 K)
Critical Pressure	532.0 psia	(3668.0 kPa [abs])
Critical Density	34.34 lb/ft^3	(550.0 kg/m^3)
Critical Volume	0.0291 ft^3/lb	(0.00182 m^3/kg)

Appendix G.1: Loop Pressure Drop MATLAB Calculations

```
% Tobin Dancy, Omesh Kamat, Tommy Larkin
% MQP
% March 21, 2016

clc; clear all;

%% Calculation - Single Phase Pressure Loss

cubicmpers_to_mlpermin = 60000000; % m^3/s to mL/min conversion
inch_to_m = 0.0254; % inches to meters conversion

% Initial Information
d_tube = 0.18 * inch_to_m; % [m]
density_R123 = 1578; % Density [kg/m^3]
mu_R123 = 0.00082; % Dynamic Viscosity [kg/m*s]
surfaceRoughness_SS = 0.000015; % [m]

fprintf('Velocity    Sect1P    Sect1FR    Sect2P    Sect2FR    Sect3P    Sect3FR    Sect4P    Sect4FR    Sect5P
Sect5FR    TotalP\n');

for velocity = 0:0.0001:0.004

    % Section 1 - Reservoir Side
    sect1_d = d_tube; % [m]
    sect1_length = 0.6; % [m]
    sect1_area = (pi/4)*sect1_d^2; % [m^2]

    sect1_Re = (density_R123*velocity*sect1_length)/mu_R123;

    if sect1_Re < 2000
        sect1_fd = 64/sect1_Re;
    else
        sect1_fd = 0.3164/(sect1_Re^0.25);
    end

    sect1_p = sect1_length*sect1_fd*(density_R123/2)*(velocity^2/sect1_d);
    sect1_flowrate = velocity*sect1_area*cubicmpers_to_mlpermin;

    % Section 2 - Mechanical Pump Side
    sect2_d = d_tube; % [m]
    sect2_length = 0.4; % [m]
    sect2_area = (pi/4)*sect2_d^2; % [m^2]

    sect2_Re = (density_R123*velocity*sect2_length)/mu_R123;

    if sect2_Re < 2000
        sect2_fd = 64/sect2_Re;
    else
        sect2_fd = 0.3164/(sect2_Re^0.25);
    end
```

```
sect2_p = sect2_length*sect2_fd*(density_R123/2)*(velocity^2/sect2_d);
sect2_flowrate = velocity*sect2_area*cubicmpers_to_mlpermin;

% Section 3 - Condenser Side
sect3_d = d_tube; % [m]
sect3_length = 0.4; % [m]
sect3_area = (pi/4)*sect3_d^2; % [m^2]

sect3_Re = (density_R123*velocity*sect3_length)/mu_R123;

if sect3_Re < 2000
   sect3_fd = 64/sect3_Re;
else
   sect3_fd = 0.3164/(sect3_Re^0.25);
end

sect3_p = sect3_length*sect3_fd*(density_R123/2)*(velocity^2/sect3_d);
sect3_flowrate = velocity*sect3_area*cubicmpers_to_mlpermin;

% Section 4 - Evaporator Side
sect4_d = d_tube; % [m]
sect4_length = 0.68; % [m]
sect4_area = (pi/4)*sect4_d^2; % [m^2]

sect4_Re = (density_R123*velocity*sect4_length)/mu_R123;

if sect4_Re < 2000
   sect4_fd = 64/sect4_Re;
else
   sect4_fd = 0.3164/(sect4_Re^0.25);
end

sect4_p = sect4_length*sect4_fd*(density_R123/2)*(velocity^2/sect4_d);
sect4_flowrate = velocity*sect4_area*cubicmpers_to_mlpermin;

% Section 5 - Evaporator
sect5_width = 0.003; % [m]
sect5_height = 0.0005; % [m]
sect5_length = 0.01; % [m]

sect5_d = (2*sect5_width*sect5_height)/(sect5_width + sect5_height);
sect5_area = (pi/4)*sect5_d^2; % [m^2]
sect5_Re = (density_R123*velocity*sect5_length)/mu_R123;

if sect5_Re < 2000
   sect5_fd = 64/sect5_Re;
else
   sect5_fd = 0.3164/(sect5_Re^0.25);
end

sect5_p = 2*(sect5_length*sect5_fd*(density_R123/2)*(velocity^2/sect5_d));
sect5_flowrate = velocity*sect5_area*cubicmpers_to_mlpermin;
```

```
    % Total
    total_p = sect1_p + sect2_p + sect3_p + sect4_p + sect5_p;


fprintf('%f\t%f\t%f\t%f\t%f\t%f\t%f\t%f\t%f\t%f\t%f\n',velocity,sect1_p,sect1_flowrate,sect2_p,sect2_flowrate,
sect3_p,sect3_flowrate,sect4_p,sect4_flowrate,sect5_p,sect5_flowrate,total_p);
end
```

Appendix G.2: Evaporator Pressure Drop MATLAB Calculations

```
% Tobin Dancy, Omesh Kamat, Tommy Larkin
% MQP
% September 28, 2015

clc;

%% Conversion Constants

sqcm_to_sqmm = 10000; % cm^2 to mm^2 Conversion
cubicmpers_to_mlpermin = 60000000; % m^3/s to mL/min Conversion

%% Initial Information

width_channel = 0.003; % Width of Channel [m]
height_channel = 0.0005; % Height of Channel [m]
length_channel = 0.01; % Length of Channel (on 10 mm chip) [m]
Ra_channel = 0.000015; % Surface Roughness of the Channel [m]
g = 9.8; % Gravity Constant [m/s^2]

flux = 10; % Heat Transfer [Watts/cm^2]
Q = flux * sqcm_to_sqmm * width_channel * length_channel; % Heat removed from 1 channel [Watts]

A_channel = width_channel * height_channel; % Area of 1 Channel [m^2]
d_hydraulic_channel = (2 * A_channel)/(width_channel + height_channel); % Hydraulic Diameter for all
calculations (rectangular duct)

A_wet_channel = (pi * (d_hydraulic_channel^2))/4; % Wetted Area of 1 Channel [m^2]

%% Fluid Properties

% R-123
rho_R123 = 1578; % Density [kg/m^3]
LH_R123 = 173000; % Latent Heat [J/kg]
mu_R123 = 0.00082; % Dynamic Viscosity [Pa/s] = [kg/(m*s)]

% Novec-7600
rho_N7600 = 1540; % Density [kg/m^3]
LH_N7600 = 115600; % Latent Heat [J/kg]
mu_N7600 = 0.001648; % Dynamic Viscosity [Pa/s] = [kg/(m*s)]

% Novec-7100
rho_N7100 = 1520; % Density [kg/m^3]
LH_N7100 = 125000; % Latent Heat [J/kg]
mu_N7100 = 0.00061; % Dynamic Viscosity [Pa/s] = [kg/(m*s)]

% Novec-7000
rho_N7000 = 1400; % Density [kg/m^3]
LH_N7000 = 142000; % Latent Heat [J/kg]
mu_N7000 = 0.000448; % Dynamic Viscosity [Pa/s] = [kg/(m*s)]
```

```
%% Calculated Values

% Velocity

m_dot_R123 = Q/LH_R123; % Mass Flow Rate for R123 [kg/s]
m_dot_N7600 = Q/LH_N7600; % Mass Flow Rate for N7600 [kg/s]
m_dot_N7100 = Q/LH_N7100; % Mass Flow Rate for N7100 [kg/s]
m_dot_N7000 = Q/LH_N7000; % Mass Flow Rate for N7000 [kg/s]

V_dot_R123_SI = m_dot_R123/rho_R123; % Volumetric Flow Rate for R123 [m^3/s]
V_dot_N7600_SI = m_dot_N7600/rho_N7600; % Volumetric Flow Rate for N7600 [m^3/s]
V_dot_N7100_SI = m_dot_N7100/rho_N7100; % Volumetric Flow Rate for N7100 [m^3/s]
V_dot_N7000_SI = m_dot_N7000/rho_N7000; % Volumetric Flow Rate for N7000 [m^3/s]

V_dot_R123 = V_dot_R123_SI * cubicmpers_to_mlpermin; % Volumetric Flow Rate for R123 [mL/min]
V_dot_N7600 = V_dot_N7600_SI * cubicmpers_to_mlpermin; % Volumetric Flow Rate for N7600 [mL/min]
V_dot_N7100 = V_dot_N7100_SI * cubicmpers_to_mlpermin; % Volumetric Flow Rate for N7100 [mL/min]
V_dot_N7000 = V_dot_N7000_SI * cubicmpers_to_mlpermin; % Volumetric Flow Rate for N7000 [mL/min]

v_R123_SI = V_dot_R123_SI/A_wet_channel; % Velocity for R123 [m/s]
v_N7600_SI = V_dot_N7600_SI/A_wet_channel; % Velocity for N7600 [m/s]
v_N7100_SI = V_dot_N7100_SI/A_wet_channel; % Velocity for N7100 [m/s]
v_N7000_SI = V_dot_N7000_SI/A_wet_channel; % Velocity for N7000 [m/s]

% Pressure Drop

Re_R123 = (v_R123_SI * d_hydraulic_channel * rho_R123)/mu_R123; % Reynolds Number for R123
Re_N7600 = (v_N7600_SI * d_hydraulic_channel * rho_N7600)/mu_N7600; % Reynolds Number for N7600
Re_N7100 = (v_N7100_SI * d_hydraulic_channel * rho_N7100)/mu_N7100; % Reynolds Number for N7100
Re_N7000 = (v_N7000_SI * d_hydraulic_channel * rho_N7000)/mu_N7000; % Reynolds Number for N7000

if (Re_R123 <= 2100)
   f_R123 = 64/Re_R123;
else
   f_R123 = 1.325/(log((Ra_channel/(3.7 * d_hydraulic_channel))+(5.74/(Re_R123^0.9)))^2);
end

if (Re_N7600 <= 2100)
   f_N7600 = 64/Re_N7600;
else
   f_N7600 = 1.325/(log((Ra_channel/(3.7 * d_hydraulic_channel))+(5.74/(Re_N7600^0.9)))^2);
end

if (Re_N7100 <= 2100)
   f_N7100 = 64/Re_N7100;
else
   f_N7100 = 1.325/(log((Ra_channel/(3.7 * d_hydraulic_channel))+(5.74/(Re_N7100^0.9)))^2);
end

if (Re_N7000 <= 2100)
   f_N7000 = 64/Re_N7000;
else
```

```
    f_N7000 = 1.325/(log((Ra_channel/(3.7 * d_hydraulic_channel))+(5.74/(Re_N7000^0.9)))^2);
end

Hf_R123 = f_R123 * (length_channel/d_hydraulic_channel) * (v_R123_SI^2/(2 * g));
Hf_N7600 = f_N7600 * (length_channel/d_hydraulic_channel) * (v_N7600_SI^2/(2 * g));
Hf_N7100 = f_N7100 * (length_channel/d_hydraulic_channel) * (v_N7100_SI^2/(2 * g));
Hf_N7000 = f_N7000 * (length_channel/d_hydraulic_channel) * (v_N7000_SI^2/(2 * g));

FS_twophase = 5;

%% Equation 1 - Pressure Drop
% Pressure Drop = density * gravity * headloss

Pdrop_EQ1_R123_SP = rho_R123 * g * Hf_R123;
Pdrop_EQ1_N7600_SP = rho_N7600 * g * Hf_N7600;
Pdrop_EQ1_N7100_SP = rho_N7100 * g * Hf_N7100;
Pdrop_EQ1_N7000_SP = rho_N7000 * g * Hf_N7000;

Pdrop_EQ1_R123_TP = Pdrop_EQ1_R123_SP * FS_twophase;
Pdrop_EQ1_N7600_TP = Pdrop_EQ1_N7600_SP * FS_twophase;
Pdrop_EQ1_N7100_TP = Pdrop_EQ1_N7100_SP * FS_twophase;
Pdrop_EQ1_N7000_TP = Pdrop_EQ1_N7000_SP * FS_twophase;

%% Equation 2 - Pressure Drop
% Pressure Drop = f * (L/D) * ((rho * velocity^2)/2)

Pdrop_EQ2_R123_SP = f_R123 * (length_channel/d_hydraulic_channel) * ((rho_R123 * v_R123_SI^2)/2);
Pdrop_EQ2_N7600_SP = f_N7600 * (length_channel/d_hydraulic_channel) * ((rho_N7600 * v_N7600_SI^2)/2);
Pdrop_EQ2_N7100_SP = f_N7100 * (length_channel/d_hydraulic_channel) * ((rho_N7100 * v_N7100_SI^2)/2);
Pdrop_EQ2_N7000_SP = f_N7000 * (length_channel/d_hydraulic_channel) * ((rho_N7000 * v_N7000_SI^2)/2);

Pdrop_EQ2_R123_TP = Pdrop_EQ2_R123_SP * FS_twophase;
Pdrop_EQ2_N7600_TP = Pdrop_EQ2_N7600_SP * FS_twophase;
Pdrop_EQ2_N7100_TP = Pdrop_EQ2_N7100_SP * FS_twophase;
Pdrop_EQ2_N7000_TP = Pdrop_EQ2_N7000_SP * FS_twophase;

%% Equation 3 - Pressure Drop
% Pressure Drop = (8 * f * rho * L * Vdot^2)/(pi * D^5)

Pdrop_EQ3_R123_SP = (8 * f_R123 * rho_R123 * length_channel * V_dot_R123_SI^2)/(pi *
d_hydraulic_channel^5);
Pdrop_EQ3_N7600_SP = (8 * f_N7600 * rho_N7600 * length_channel * V_dot_N7600_SI^2)/(pi *
d_hydraulic_channel^5);
Pdrop_EQ3_N7100_SP = (8 * f_N7100 * rho_N7100 * length_channel * V_dot_N7100_SI^2)/(pi *
d_hydraulic_channel^5);
Pdrop_EQ3_N7000_SP = (8 * f_N7000 * rho_N7000 * length_channel * V_dot_N7000_SI^2)/(pi *
d_hydraulic_channel^5);

Pdrop_EQ3_R123_TP = Pdrop_EQ3_R123_SP * FS_twophase;
Pdrop_EQ3_N7600_TP = Pdrop_EQ3_N7600_SP * FS_twophase;
Pdrop_EQ3_N7100_TP = Pdrop_EQ3_N7100_SP * FS_twophase;
Pdrop_EQ3_N7000_TP = Pdrop_EQ3_N7000_SP * FS_twophase;
```

```
%% Display Information

% Constant Values
fprintf('Constant Values for All Calculations \n\n');
fprintf('Channel Width [m]: %f\n', width_channel);
fprintf('Total Heat Removed [W] - Based on width since flux must be 10 W/cm^2: %f\n', Q);
fprintf('Channel Hydraulic Diameter [m]: %e\n', d_hydraulic_channel);
fprintf('Channel Area: %e\n', A_channel);
fprintf('Channel Wetted Area: %e\n', A_wet_channel);

% R123
fprintf('R-123 Calculated Values \n\n');
fprintf('Mass Flow Rate [kg/s]: %f\n', m_dot_R123);
fprintf('Volumetric Flow Rate [m^3/s]: %e\n', V_dot_R123_SI);
fprintf('Volumetric Flow Rate [mL/min]: %e\n', V_dot_R123);
fprintf('Velocity [m/s]: %f\n', v_R123_SI);
fprintf('Reynolds Number: %f\n', Re_R123);
fprintf('Friction Factor: %f\n', f_R123);
fprintf('Headloss [Pa]: %e\n', Hf_R123);
fprintf('Pressure Drop (Equation 1) [Pa] - Single Phase: %e\n', Pdrop_EQ1_R123_SP);
fprintf('Pressure Drop (Equation 2) [Pa] - Single Phase: %e\n', Pdrop_EQ2_R123_SP);
fprintf('Pressure Drop (Equation 3) [Pa] - Single Phase: %e\n', Pdrop_EQ3_R123_SP);
fprintf('Pressure Drop (Equation 1) [Pa] - Two Phase: %e\n', Pdrop_EQ1_R123_TP);
fprintf('Pressure Drop (Equation 2) [Pa] - Two Phase: %e\n', Pdrop_EQ2_R123_TP);
fprintf('Pressure Drop (Equation 3) [Pa] - Two Phase: %e\n', Pdrop_EQ3_R123_TP);

% N7600
fprintf('N7600 Calculated Values \n\n');
fprintf('Mass Flow Rate [kg/s]: %f\n', m_dot_N7600);
fprintf('Volumetric Flow Rate [m^3/s]: %e\n', V_dot_N7600_SI);
fprintf('Volumetric Flow Rate [mL/min]: %e\n', V_dot_N7600);
fprintf('Velocity [m/s]: %f\n', v_N7600_SI);
fprintf('Reynolds Number: %f\n', Re_N7600);
fprintf('Friction Factor: %f\n', f_N7600);
fprintf('Headloss [Pa]: %e\n', Hf_N7600);
fprintf('Pressure Drop (Equation 1) [Pa] - Single Phase: %e\n', Pdrop_EQ1_N7600_SP);
fprintf('Pressure Drop (Equation 2) [Pa] - Single Phase: %e\n', Pdrop_EQ2_N7600_SP);
fprintf('Pressure Drop (Equation 3) [Pa] - Single Phase: %e\n', Pdrop_EQ3_N7600_SP);
fprintf('Pressure Drop (Equation 1) [Pa] - Two Phase: %e\n', Pdrop_EQ1_N7600_TP);
fprintf('Pressure Drop (Equation 2) [Pa] - Two Phase: %e\n', Pdrop_EQ2_N7600_TP);
fprintf('Pressure Drop (Equation 3) [Pa] - Two Phase: %e\n', Pdrop_EQ3_N7600_TP);

% N7100
fprintf('N7100 Calculated Values \n\n');
fprintf('Mass Flow Rate [kg/s]: %f\n', m_dot_N7100);
fprintf('Volumetric Flow Rate [m^3/s]: %e\n', V_dot_N7100_SI);
fprintf('Volumetric Flow Rate [mL/min]: %e\n', V_dot_N7100);
fprintf('Velocity [m/s]: %f\n', v_N7100_SI);
fprintf('Reynolds Number: %f\n', Re_N7100);
fprintf('Friction Factor: %f\n', f_N7100);
fprintf('Headloss [Pa]: %e\n', Hf_N7100);
fprintf('Pressure Drop (Equation 1) [Pa] - Single Phase: %e\n', Pdrop_EQ1_N7100_SP);
fprintf('Pressure Drop (Equation 2) [Pa] - Single Phase: %e\n', Pdrop_EQ2_N7100_SP);
fprintf('Pressure Drop (Equation 3) [Pa] - Single Phase: %e\n', Pdrop_EQ3_N7100_SP);
fprintf('Pressure Drop (Equation 1) [Pa] - Two Phase: %e\n', Pdrop_EQ1_N7100_TP);
```

```
fprintf('Pressure Drop (Equation 2) [Pa] - Two Phase: %e\n', Pdrop_EQ2_N7100_TP);
fprintf('Pressure Drop (Equation 3) [Pa] - Two Phase: %e\n', Pdrop_EQ3_N7100_TP);

% N7000
fprintf('N7000 Calculated Values \n\n');
fprintf('Mass Flow Rate [kg/s]: %f\n', m_dot_N7000);
fprintf('Volumetric Flow Rate [m^3/s]: %e\n', V_dot_N7000_SI);
fprintf('Volumetric Flow Rate [mL/min]: %e\n', V_dot_N7000);
fprintf('Velocity [m/s]: %f\n', v_N7000_SI);
fprintf('Reynolds Number: %f\n', Re_N7000);
fprintf('Friction Factor: %f\n', f_N7000);
fprintf('Headloss [Pa]: %e\n', Hf_N7000);
fprintf('Pressure Drop (Equation 1) [Pa] - Single Phase: %e\n', Pdrop_EQ1_N7000_SP);
fprintf('Pressure Drop (Equation 2) [Pa] - Single Phase: %e\n', Pdrop_EQ2_N7000_SP);
fprintf('Pressure Drop (Equation 3) [Pa] - Single Phase: %e\n', Pdrop_EQ3_N7000_SP);
fprintf('Pressure Drop (Equation 1) [Pa] - Two Phase: %e\n', Pdrop_EQ1_N7000_TP);
fprintf('Pressure Drop (Equation 2) [Pa] - Two Phase: %e\n', Pdrop_EQ2_N7000_TP);
fprintf('Pressure Drop (Equation 3) [Pa] - Two Phase: %e\n', Pdrop_EQ3_N7000_TP);
```

Appendix G.3: Length of Condenser MATLAB Calculations

```
% MQP Calculations
% Tobin Dancy, Omesh Kamat, Tommy Larkin
% January 18, 2015

clear all; clc;

x = 0;

while x == 0
   %% Length of Condenser
   prompt = 'What temperature do you want want the condenser to be? [Celsius]: ';
   outsideTemp = 273.15 + input(prompt);

   rho_R123 = 1471.5; %[kg/m^3]
   roomTemp = 294.26; %[K]
   boilingTemp = 300.97; %[K]
   insideRadius = 0.004572; %[m]
   outsideRadius = 0.00635; %[m]

   % Heat Added in Evaporator
   length_Evaporator = 0.01; %[m]
   width_Evaporator = 0.003; %[m]
   height_Evaporator = 0.0005; %[m]
   hVaporization_R123 = 394700; %[J/kg]

   V_Evaporator = 2*length_Evaporator*width_Evaporator*height_Evaporator;

   Q_Evaporator = rho_R123*V_Evaporator*hVaporization_R123;

   % Heat Removed from Condenser
   insideTemp = 300.97; %[K]
   thermalConductivity_Pipe = 16; %[W/m*K]
   thermalConductivity_Ice = 2.22;
   tempChange = insideTemp - outsideTemp;

   %%% Conduction
   radiusRatio = outsideRadius/insideRadius;

   Resistance1 = 1/(2*pi*thermalConductivity_Pipe)*log(radiusRatio);

   %%% Convection of Environment
   Nusselt = 3.66;

   h1 = (Nusselt*thermalConductivity_Ice)/(outsideRadius*2);
   A2 = 2*pi*outsideRadius;

   Resistance2 = 1/(h1*A2);

   Q_Condenser = tempChange/(Resistance1 + Resistance2);
```

```
    % Length of Condenser
    safetyFactor = 3;

    lengthCondenser_SI = (safetyFactor)*(Q_Evaporator/Q_Condenser);
    m_to_in_conversion = 39.3701;
    lengthCondenser_EN = lengthCondenser_SI*m_to_in_conversion;

    % Display Answers
    fprintf('\nQ_Evaporator: %f, Q_Condenser: %f, Condenser Length [m]: %f, Condenser Length [in]: %f \n',
Q_Evaporator, Q_Condenser, lengthCondenser_SI, lengthCondenser_EN);

end
```